



HAL
open science

Novel Portland cement matrices incorporating a gamma -MnO₂ /Ag₂O hydrogen/tritium getter -structure changes and trapping performance

Sandy Lanier, Catherine Davy, Cyrille Albert-Mercier, Oriane Farcy, Céline
Cau-Dit-Coumes, David Lambertin

► To cite this version:

Sandy Lanier, Catherine Davy, Cyrille Albert-Mercier, Oriane Farcy, Céline Cau-Dit-Coumes, et al..
Novel Portland cement matrices incorporating a gamma -MnO₂ /Ag₂O hydrogen/tritium getter -
structure changes and trapping performance. Journal of Nuclear Materials, 2022, Journal of Nuclear
Materials, 567, pp.153819. 10.1016/j.jnucmat.2022.153819 . hal-04044334

HAL Id: hal-04044334

<https://hal.univ-lille.fr/hal-04044334>

Submitted on 22 Jul 2024

HAL is a multi-disciplinary open access archive for the deposit and dissemination of scientific research documents, whether they are published or not. The documents may come from teaching and research institutions in France or abroad, or from public or private research centers.

L'archive ouverte pluridisciplinaire **HAL**, est destinée au dépôt et à la diffusion de documents scientifiques de niveau recherche, publiés ou non, émanant des établissements d'enseignement et de recherche français ou étrangers, des laboratoires publics ou privés.



Distributed under a Creative Commons Attribution - NonCommercial 4.0 International License

1 **Novel Portland cement matrices**
2 **incorporating a γ -MnO₂/Ag₂O hydrogen/tritium getter -**
3 **Structure changes and trapping performance**

4 S. Lanier¹, C. A. Davy^{1,*}, C. Albert-Mercier², O. Farcy³, C. Cau Dit Coumes³, D. Lambertin³

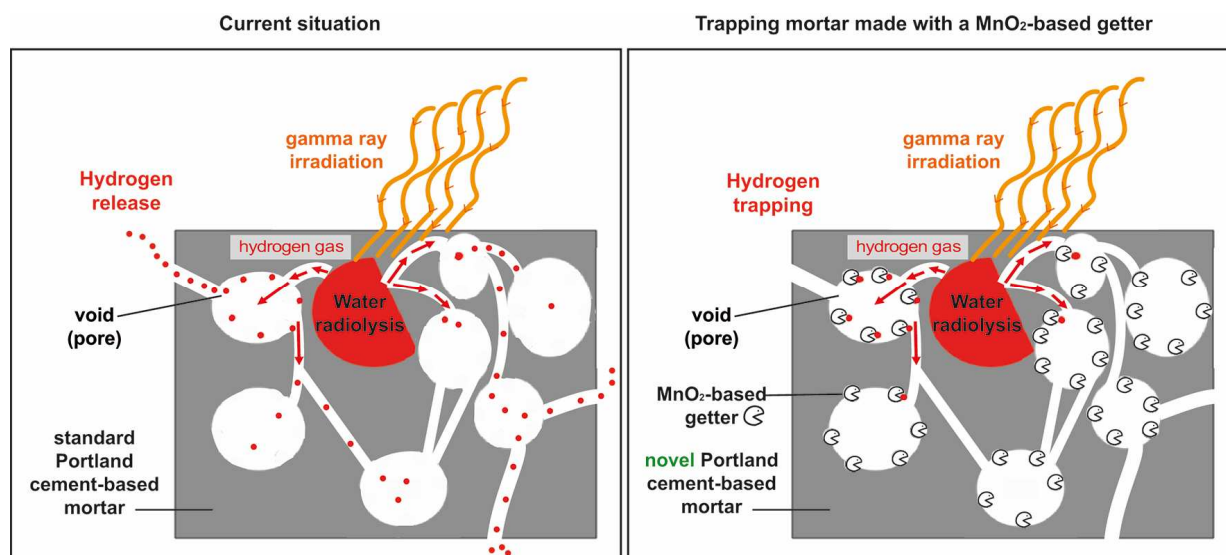
5
6 1 : Univ. Lille, CNRS, Centrale Lille, Univ. Artois, UMR 8181 – UCCS – Unité de Catalyse et
7 Chimie du Solide, F-59000 Lille, France

8 2 : Université Polytechnique Hauts-de-France, CERAMATHS, Valenciennes, France

9 3 : CEA, DES, ISEC, DE2D, Univ Montpellier, Marcoule, France

10 * Corresponding author, email: catherine.davy@centralelille.fr

11 **Graphical Abstract:**



12
13

1 **Abstract**

2 This study investigates novel Portland cement-based mortars, developed for
3 hydrogen/tritium trapping and radioactive waste immobilization. They incorporate a γ -
4 $\text{MnO}_2/\text{Ag}_2\text{O}$ getter powder at 10% wt (i.e. 6.8 to 7.1% vol). Compared to former patented
5 materials, no drying or heat treatment of the materials is needed.

6 Complementarily to X Ray Diffractometry (XRD) and thermo-gravimetry analysis (TGA), ^{27}Al
7 and ^{29}Si Magic Angle Spinning Nuclear Magnetic Resonance (MAS NMR) evidences that the
8 structure of the Portland cement solids (i.e. the C-A-S-H) is not impacted by the presence of
9 getter, even after several month curing. Yet, Scanning Electron Microscopy coupled to
10 Energy Dispersive Spectroscopy (SEM+EDS) shows that calcium is significantly present at the
11 surface of the getter grains; this could affect trapping efficiency.

12 However, after gamma irradiation with cumulated doses of 491 or 997 kGy (i.e. 23 to 46
13 days at $900 \text{ Gy}\cdot\text{h}^{-1}$), all mortars made with getter have a hydrogen trapping efficiency of
14 between 77 and 96%, when compared to the irradiation of mortars made with a non-
15 trapping $\gamma\text{-MnO}_2$ powder, or to the irradiation of pure water considered alone.

16 This means that the developed mortars display excellent hydrogen trapping efficiency,
17 without any impact on their solid structure.

18

19 **Keywords:** Portland cement; radioactive waste; trapping; tritium; getter; Hydrogen fires and
20 explosions; Hydrogen suppression

21

1	Table of contents	
2		
3	1 INTRODUCTION	5
4	1.1 Industrial context	5
5	1.2 Scientific background	6
6	1.3 Aims and scopes	8
7	2 MATERIALS AND METHODS	10
8	2.1 Materials	10
9	2.1.1 Raw powders.....	10
10	2.1.2 Mortars and pastes	11
11	2.2 Characterization methods	13
12	2.2.1 Structure characterization of the cement pastes	14
13	2.2.2 Hydrogen trapping performance: <i>in situ</i> gamma irradiation experiments.....	15
14	3 RESULTS AND DISCUSSION	18
15	3.1 Interactions between Portland cement pastes and γ-MnO₂ or γ-MnO₂/Ag₂O getter	19
16	3.1.1 XRD results	19
17	3.1.2 TGA analysis	20
18	3.1.3 ²⁹ Si MAS NMR results.....	20
19	3.2 SEM observations of the getter embedded in a Portland cement mortar	23
20	3.3 Hydrogen trapping efficiency of the Portland cement-based mortars	24
21	3.3.1 Gas production after gamma ray irradiation	25
22	3.3.2 Hydrogen production – comparison with the literature.....	25
23	3.3.3 Hydrogen trapping efficiency.....	29
24	3.3.4 Changes in mortar microstructure after gamma ray irradiation	30
25	4 CONCLUSIONS	32
26	ACKNOWLEDGMENTS	34
27	APPENDICES	35
28	A.1- Materials (complements)	35
29	A.2- Classical characterization methods	37
30	A.3 Experimental protocol for gamma irradiation measurements	39
31	REFERENCES	41
32		

1 Introduction

2 1.1 Industrial context

3 In a number of industrialized countries, particularly in the USA and in France,
4 significant amounts of the electrical energy supply are provided by the nuclear industry,
5 which uses the nuclear fission of ^{235}U in pressurized or boiling water reactors ¹. Due to this
6 activity, radioactive waste is generated every year, with 90.9 %vol short-lived and very low
7 (to low) activity compounds [ANDRA 2009, ANDRA 2018].

8 Currently, the safe conditioning of these hazardous waste includes
9 stabilization/solidification in Portland cement-based materials, which are a robust and
10 economically viable solution [Ojavan 2005, Shi 2006, AIEA2007, LeCaer 2017]. Alternatives
11 exist for specific applications, where Portland cements are inadequate, e.g. magnesium
12 potassium phosphate cements or calcium aluminate phosphate cements for the
13 immobilization of aluminum [Kinoshita 2013, CauDitCoumes 2014, Wang 2020], and
14 geopolymers for the solidification/stabilization of organic liquids [Cantarel 2015, Davy 2018]
15 or magnesium alloys [Lambertin 2012].

16 Nuclear radioactive wastes are radiation emitters of various energy and type. Their
17 ionizing rays (of either α , β or γ type) interact with the surrounding water (from the disposal
18 site or from the cement conditioning matrix), generating hydrogen (and other products) due
19 to a range of radiolysis reactions [Bouniol 2008; Varlakov 2021]. Hydrogen gas may also be
20 released by metal corrosion in the alkaline porewater of Portland-cement materials
21 [CauDitCoumes 2014]. Whenever hydrogen gas is released by a radioactive (and/or metallic)

¹ According to the International Energy Agency, in 2019 in the US, an amount of 843 330 GWh electricity has been produced from nuclear power (it is the 3rd electrical energy source, with 1,634,595 GWh from natural gas and 1,058,637 GWh from coal), see :
<https://www.iea.org/data-and-statistics/data-tables?country=USA&energy=Electricity&year=2019>.

1 waste immobilized in a cement matrix, its pressure may build up and eventually reach the
2 4 %vol flammability limit in air [Murugesan 2013] associated to an ignition energy of only
3 0.03 mJ [Zhong 2014, Wang 2020], so that the triggering conditions for hydrogen explosion
4 may be easily satisfied. Hydrogen release can thus raise important safety issues. This justifies
5 strict regulations concerning the gas release of cemented waste packages sent to disposal
6 [Lambertin 2010].

7 Apart from hydrogen gas, tritium gas, an isotope of hydrogen of 3 amu, is released by wastes
8 from current fission nuclear reactors, and significantly more will be produced in the near
9 future by the nuclear fusion reactor ITER. The latter is under construction in France by a
10 worldwide collaboration spanning 35 countries [ANDRA 2018, ASN 2010].

11

12 In France, the authorized radioactive waste repositories are managed by ANDRA
13 (Agence Nationale pour la gestion des Déchets RAdioactifs). For the main CSA near-surface
14 repository (Soulaines-Dhuys, Aube), current specifications limit the tritium outgassing rate of
15 waste packages below 2.105 Bq per ton of package and per day, considering all possible
16 gaseous forms of tritium [ANDRA 2015]. This is so restrictive that in practice, most tritiated
17 waste packages are excluded from the CSA repository, and currently stored in interim
18 facilities. Tritiated waste need to be accepted for repository in greater amounts than what is
19 currently feasible. This situation is similar to that of other industrialized countries managing
20 tritiated waste.

21 **1.2 Scientific background**

22 Although cement-based matrices are a viable option for the immobilization of
23 hydrogen or tritium-releasing nuclear waste, without peculiar precautions, and whatever
24 their formulation, they release significant amounts of H₂ gas (and other radiolytic products)

1 under varied ionizing rays, due to radiolysis reactions [Mockel1982, Bouniol 2008,
2 LeCaer2017, Acher 2018, Chartier2018, Varlakov 2021]. The international patent [Lambertin
3 2010] shows that significant trapping of H₂ is possible in cement matrices, provided that they
4 include a dedicated hydrogen-tritium getter.

5 This getter is a mix of γ -MnO₂ and Ag₂O, aimed at irreversibly trapping gaseous H₂ [Kozawa
6 1980, Kozawa 1981a, Kozawa 1981b, Galliez 2012] and its isotopes (deuterium and tritium
7 forms). Unlike other hydrogen scavengers such as polymeric compounds, metal hydrides or
8 oxides [Nigrey 2000, Chaudron 1998, Lambertin 2010], the γ -MnO₂/Ag₂O getter is neither
9 pyrophoric (i.e. with a high inflammation risk) nor sensitive to ionizing rays [Lousot 2006;
10 Chlique 2015]. Apart from hydrogen, independent research has proven its ability to trap
11 tritium gas [Janberg 1995].

12 Like other getter and trapping sorbent types [Asmussen 2018, Martin 2019], the γ -
13 MnO₂/Ag₂O getter may be incorporated in cement-based matrices. [Lambertin 2010]
14 describe a pure Portland-cement based paste incorporating the γ -MnO₂/Ag₂O getter, but
15 requiring 60°C drying. Despite excellent trapping performance (120 cm³/g after 40 days
16 under pure H₂ compared to 196 cm³/g for the dry getter considered alone), this thermal
17 treatment makes the cement matrix difficult to implement at the industrial scale relevant for
18 nuclear waste disposal.

19 Although the best trapping performance of the γ -MnO₂/Ag₂O mix is achieved in the dry state
20 [Kozawa 1981b], in proportions of 87 %wt γ -MnO₂ / 13 %wt Ag₂O [Galliez 2015], significant
21 trapping is also achieved in the partially water-saturated state. For instance, in [Kozawa
22 1981b], for the same γ -MnO₂/Ag₂O mix, 22 cm³ H₂ are trapped when the mix includes 20%
23 water, compared to 39 cm³ H₂ trapped by a mix dried at 75°C.

24 1.3 Aims and scopes

1 For a safe disposal of hydrogen- or tritium- generating radioactive waste, it is
2 compulsory to have cement-based matrices 1) adapted to immobilize hydrogen or tritium-
3 releasing waste, i.e. (for instance) incorporating the γ -MnO₂/Ag₂O getter, and 2) adapted to
4 industrial uses, i.e. not requiring any heat treatment and compliant with ANDRA industrial
5 specifications.

6 In earlier research [Lanier 2020], such mortars have been designed based on pure and
7 composed Portland cements (Type I and Type V). They incorporate a fixed amount of 10% γ -
8 MnO₂/Ag₂O getter in a powdered form (expressed in % of the total mortar mass). Their
9 curing is endogenous, and no heat treatment is performed.

10 The trapping efficiency of these novel developed mortars is assessed in this study,
11 because of potential detrimental interactions between the γ -MnO₂/Ag₂O getter and the
12 Portland cement paste (mainly the porewater and the Calcium Aluminate and Silicate
13 Hydrates i.e. the C-A-S-H², see [Geng 2017]). In particular, a significant cation sorption on δ -
14 MnO₂, such as Ca²⁺, has been identified by [Pretorius 2001]. This phenomenon, if occurring
15 for the γ -MnO₂/Ag₂O getter present in the partially water-saturated Portland cement-based
16 mortars, may significantly hinder their hydrogen trapping efficiency.

17 Following the promising mortars developed in [Lanier 2020], this contribution
18 investigates first, what interactions exist between the γ -MnO₂/Ag₂O getter and the Portland
19 cement solids or its porewater, by combining (1) X Ray Diffraction (XRD), thermogravimetry

² For the sake of simplicity, in this research, the main solid components of hydrated Portland-based cements, which incorporate calcium silicates, are referred to as C-A-S-H (Calcium Aluminate and Silicate Hydrates), but in pure Portland (Type I) cement, aluminates are almost absent, so that a more adequate term would be Calcium Silicate Hydrates (C-S-H). However, there are actual C-A-S-H in composed Portland cements, such as in the Type V also used herein.

1 (TGA) analysis, ^{27}Al and ^{29}Si Magic Angle Spinning Nuclear Magnetic Resonance (MAS NMR)
2 for the interactions between the cement solids and the getter, and (2) SEM/EDS (Scanning
3 Electron Microscopy/Energy Dispersive Spectroscopy) of the getter powder embedded in a
4 hardened mortar.

5 Secondly, the H_2 trapping performance is investigated for the novel mortars incorporating
6 the $\gamma\text{-MnO}_2/\text{Ag}_2\text{O}$ getter, and compared to mortars made with non-trapping $\gamma\text{-MnO}_2$ only.
7 Gamma Ray irradiation experiments are performed on mortar samples placed in an inert
8 argon gas atmosphere, after 4 months curing and without preliminary drying or heat
9 treatment. Gamma Ray irradiation generates *in situ* radiolysis of the water present in the
10 mortars [Acher 2018]. This in turn creates mainly hydrogen gas, that the getter may or may
11 not trap. Finally, SEM observations and nitrogen sorption-desorption measurements are
12 performed before and after irradiation, in order to analyze the changes in the mortar
13 structure.

14

2 Materials and Methods

2.1 Materials

2.1.1 Raw powders

All materials are made either with Type I (pure) Portland cement or with Type V (composed) Portland cement. Detailed cement references are given in Appendix A.1. According to its technical specifications, Type V cement is a mix of 53% clinker, 3% gypsum, 22% fly ash and 22% blast furnace slag. Contrarily to Type I cement, the pozzolanic and hydraulic supplementary materials (i.e. fly ash and blast furnace slag) of Type V cement avoid cement paste carbonation [Baroghel-Bouny 1994]. The chemical composition of both cements, determined by X Ray Fluorescence (XRF), is given in Table 1. Their particle size distribution (PSD) is given in Fig. 1, and shown to be similar to that of γ -MnO₂ and γ -MnO₂/Ag₂O getter. These PSD are determined by morpho-granulometry on a MorphologiG3 apparatus (Malvern Panalytical, Netherlands and UK).

Mortars are made by using specifically designed grain size classes of a standard pure silica sand (see Appendix A.1. for more information).

The γ -MnO₂/Ag₂O getter is provided by A3I (France). A commercial Manganese (IV) oxide γ -MnO₂ powder is used (reference n. 8.05958.1000, Merck, USA). Although it is slightly finer, γ -MnO₂ has a particle size distribution close to that of the γ -MnO₂/Ag₂O powder (Fig. 1). With the selected mortar formulations, γ -MnO₂ is used as a non-trapping powder, in order to quantify (by comparison) the trapping performance of mortars incorporating the γ -MnO₂/Ag₂O getter, without changing the mortar microstructure. From XRF measurements,

1 Table 1 shows the high purity of γ -MnO₂ and γ -MnO₂/Ag₂O powders. More elements on
2 powder and sand characterization are given in Appendix A.1.

3 2.1.2 Mortars and pastes

4 2.1.2.1- Reference material

5 The Portland cement paste described in [Lambertin 2010], labelled PASTE-REF-CEMI, is made
6 with a composition given in Table 2. Details on its manufacturing process and curing
7 conditions are given in Appendix A.1.

8 2.1.2.2- Hydrogen trapping mortars

9 For formulation and characterization purposes, unless otherwise stated, γ -MnO₂ is used
10 instead of the more expensive γ -MnO₂/Ag₂O getter. The getter powder is only mixed in
11 mortars for the gamma irradiation experiments and SEM observations (see below).

12 Two mortars are labelled TER-, meaning that they incorporate two main grain size classes of
13 silica sand and powdered γ -MnO₂ (or γ -MnO₂/Ag₂O); they mainly differ by the cement nature
14 (Type I or Type V) and the W/C ratio; they are labelled TER-I 54 TER-V-48 (where I or V
15 stands for the type of cement, and 54 or 48 is the water-to-cement ratio W/C multiplied by
16 one hundred).

17 A third formulation is labelled QUAT-V-48 (where V stands for Type V cement and 48 is a
18 hundred times the W/C ratio), for quaternary mortar. In that case, apart from incorporating
19 two grain classes of silica sand, the (γ -MnO₂ or γ -MnO₂/Ag₂O) powder is partially used after a
20 granulation step. The granules are a mix of cement, powder and water; they are
21 manufactured, subjected to endogenous curing for 7 days and selected (by sieving) for their
22 size; granules display significant porosity, which increases the pore volume available to gas.

1 In order to fulfill the industrial specifications, the γ -MnO₂ (or γ -MnO₂/Ag₂O) is used both as
2 granules and powder in the QUAT-V-48 formulation.

3 The composition of the three developed trapping mortars and their fresh state properties
4 (spread and Vicat setting time) are given in Table 2. Note that all three mortars contain very
5 close water proportions and identical γ -MnO₂ (or γ -MnO₂/Ag₂O) amounts. A 10% mass
6 proportion of γ -MnO₂ (or γ -MnO₂/Ag₂O) corresponds to 6.8 to 7.1% of the mortar total
7 volume depending on the formulation considered (Table 2). This means that no percolation-
8 type cluster, expected from 15% vol, may develop and change the wasteform properties
9 [Juoi 2008, Ojovan 2005].

10 The W/C ratio for each mortar is chosen as the smallest possible while complying with the
11 industrial specifications (in particular, a minimum ASTM spread of 20 cm), while maximizing
12 compressive strength and minimizing fluid transport properties.

13 2.1.2.3- Mortar manufacturing and maturation

14 For all mortars, the mixing procedure is carried out in accordance with standard EN 196-1.
15 For pore structure assessment, cylindrical molds of 65 mm by diameter and 10-15 mm by
16 height are filled with fresh mortar, sealed and cured at ambient temperature (21°C +/-1) for
17 127 days (4 months and a half). This duration is chosen in order to have a maturation close
18 to that of samples subjected to irradiation tests (see Table 3).

19 For gamma irradiation tests, reference mortars are made with γ -MnO₂ powder or with a mix
20 of γ -MnO₂ powder and granules, for the three formulations TER-I 54, TER-V 48 and QUAT-V
21 48. Hydrogen trapping mortars with the same formulations are made using γ -MnO₂/Ag₂O
22 getter. For each formulation and powder type (γ -MnO₂ or getter), four samples are made by
23 pouring the fresh paste into sealed tubes of 15 mL, corresponding to an individual sample

1 mass of 22.5 g +/-1.4. After endogenous curing at ambient temperature (21°C +/-1), gamma
2 Ray irradiation starts after 115-118 days (i.e. 4 months) maturation, and ends at an age of
3 138-164 days (i.e. 5-6 months) depending on the cumulated dose applied (Table 3).

4 2.1.2.4- Paste manufacturing, curing and drying

5 In order to avoid the shadowing effects of sand presence, chemical characterizations are
6 performed on Type I and Type V cement pastes made at W/C=0.50 and 0.54 (for Type I
7 cement) and 0.48 and 0.50 (for Type V cement). Using a common W/C=0.50 allows more
8 accurate comparison between Type I and Type V cement pastes than only 0.54 or 0.48 (used
9 for the mortars).

10 For XRD, TGA and MAS NMR experiments, after 127 days (i.e. 4,5 months) endogenous
11 curing at a constant ambient temperature of 21°C +/-1, each paste sample is dried by the
12 solvent exchange technique (with isopropanol) [Konecny 1993; Korpa 2006; Zhang and
13 Scherer 2011; Stephant 2015; Lahalle 2016] and powdered manually using a mortar and
14 pestle. Further details on paste preparation prior to characterization tests are provided in
15 Appendix A.1.

16 The age and characteristics of the irradiated samples is given in Table 3. The samples tested
17 after irradiation by nitrogen sorption-desorption and SEM are those retrieved after the
18 irradiation experiment (Table 6); their age is that given in Table 3 (i.e. 138-164 days
19 depending on the cumulated dose).

1 2.2 Characterization methods

2 For each mortar, classical protocols are used to characterize their pore size distribution and
3 porosity, before and/or after irradiation (nitrogen sorption-desorption isotherms, ethanol
4 saturation). These are detailed in Appendix A.2. With these methods, different non
5 irradiated (NI) and irradiated (IR) mortar samples are characterized at the same age.

6 The procedure for Scanning Electron Microscopy (SEM) observations of the mortars is also
7 described in Appendix A.2.

8 2.2.1 Structure characterization of the cement pastes

9 Cement paste characterization includes thermogravimetry analysis (TGA). Its protocol is
10 given in Appendix A.2.

11 2.2.1.1- XRD analysis

12 Qualitative diffraction data are collected at room temperature with a Bragg-Brentano
13 diffractometer in the θ/θ geometry (Bruker Advance D8 type), equipped with a lynx-eye
14 detector, and using copper Cu $K\alpha_1$ and $K\alpha_2$ radiations ($\lambda = 1.54060$ and 1.54440 Å, at 40.0 kV
15 and 40.0 mA), in the 2θ range from 10 to 70°, with 0.03° steps and 4 s acquisition time per
16 step. The energy discrimination of the detector is adapted in order limit fluorescence (due to
17 the presence of Mn in the specimens).

18 2.2.1.2- MAS NMR measurements

19 For ^{29}Si , the experiments are performed at a Larmor frequency of 79.5 MHz, on a 9.4 T
20 Bruker Avance 400 MHz spectrometer. In order to identify the silicate Q^n speciation (where n
21 is the number of bridging oxygen atoms of the silicate under investigation), ^{29}Si MAS-NMR
22 spectra are recorded on a 7 mm probe head with a spinning frequency (n_{rot}) of 5 kHz, a 6 μs
23 pulse length (and 90° pulse angle), 128 to 1400 transients (depending on the sample

1 considered) and an optimized recycle delay (rd) of 20 s (D1). The ²⁹Si chemical shifts are
2 referred to a TetraMethylSilane (TMS) solution as 0 ppm value.

3 ²⁷Al spectra are acquired on a Bruker Avance II 800 MHz (18.8 T) apparatus at a Larmor
4 frequency of 208.5 MHz, with a 3.2 mm zircon probe head. The spinning frequency is of
5 22 kHz, the pulse length of 0.55 μs, the pulse angle of π/10, the optimized recycle delay of 1
6 s (D1), and the number of transients is of 2048. The ²⁷Al chemical shifts are calibrated with a
7 Al(H₂O)₆³⁺ solution.

8 After acquisition, all spectra are decomposed using the DMFIT software [Massiot 2002]. This
9 provides the relative proportions of the different components of the spectra, particularly of
10 the Qⁿ silicate units (where n varies between 1 and 4, with or without Al substitutions).

11 For the ²⁹Si spectra, the mean C-A-S-H chain length is calculated according to [Richardson
12 1999]:

$$13 \quad MCL = \text{Mean Chain Length} = [2 * (Q^1 + Q^2 + \frac{3}{2} * Q^2(Al))] / Q^1$$

14 The (Al/Si) molar ratio of the C-A-S-H, i.e. the substitution rate of silicates by aluminates, is
15 also calculated using [Richardson 1994], [Andersen 2004] as:

$$16 \quad Al/Si = \frac{1}{2} Q^2(Al) / (Q^1 + Q^2 + Q^2(Al))$$

17 2.2.2 Hydrogen trapping performance: *in situ* gamma irradiation experiments

18 In this research, prior to irradiation, each sample is sealed in a glass vial under an inert argon
19 atmosphere, at a pressure slightly smaller than atmospheric pressure. No interaction with
20 ambient air exists.

1 Gamma irradiation experiments generate *in situ*, i.e. within the mortars, a number of
2 radiolytic products, including gaseous H₂ mainly from the free or bound water present, due
3 to water radiolysis [Bouniol 2008; Acher 2018]. Whenever the γ -MnO₂/Ag₂O getter is
4 present, it is expected that H₂ is irreversibly trapped and less gas is released from the
5 mortars. Other gases may also be produced, mainly O₂, CO₂, CH₄ or N₂, e.g. due to super-
6 plasticizer degradation under gamma ray action [Chartier 2018].

7 The protocol for external gamma irradiation is presented in Fig. 2. It is identical to that
8 described in [Chartier 2018]. All experiments are performed at room temperature, with an
9 average dose rate of 900 Gy.h⁻¹ and an integrated dose of 491.2 or 997.5 kGy. This
10 represents 23 or 46 days of gamma ray irradiation. All samples are monoliths (i.e. not
11 crushed or powdered mortars). Two different samples per dose and per mortar formulation
12 (either made with γ -MnO₂ or with γ -MnO₂/Ag₂O) are tested. The greatest cumulated dose
13 corresponds to the order of magnitude of the dose in [Mobasher 2015] (4.77 MGy over 11
14 days) for a slag cement-based grout used for encapsulation of low and intermediate level
15 radioactive waste. Further details on the test set-up and gas measurement apparatus are
16 given in Appendix A.3.

17 From the raw measurement of gas volume percentage in the airtight test vial (%*vol*) (by gas
18 micro-chromatography), the amount of gas $n(\text{gas})$ (in mol) is deduced from the gas perfect
19 law, and the corresponding gas radiolytic yield of the considered sample $G(\text{gas})_{\text{material}}$ is
20 calculated (see Appendix A.3.). In this research, only nitrogen gas is detected together with
21 H₂. Due to the amounts produced, only $G(\text{H}_2)_{\text{material}}$ is discussed. The radiolytic yield for
22 other produced gaseous species is not accounted for.

1 Because water is the main significant source of H₂ in the mortars, the hydrogen radiolytic
 2 yield is rather expressed (in mol/J) after being normalized by the mass water fraction w_{water}
 3 as:

$$4 \quad \frac{G(H_2)_{material}}{w_{water}} = \frac{n(H_2)}{D m_{total\ water}}$$

5 Where $w_{water} = m_{total\ water}/m$ and $m_{total\ water}$ is the total water mass inside the sample,
 6 both free and bound; m is the sample mass.

7 The measurements are generally compared to the radiolytic yield of free water. It is not easy
 8 to assess this value experimentally because H₂ recombines easily to form water molecules
 9 [LaVerne 2009; Chartier 2017]. In presence of H₂ trapping compounds (such as Br⁻ ions),
 10 [LaVerne 2009] determined a radiolytic yield for free water at a value of 4.46×10^{-8} mol/J.
 11 This value is used as a reference (labelled free or pure water) in this research.

12 The amount of H₂ generated by free water is a theoretical value $n(H_{2\ free\ water})$ (expressed
 13 in mol). It is calculated using the actual amount of water present in each mortar formulation
 14 (i.e. both free and bound water), as in [Chartier 2017], by:

$$15 \quad n(H_{2\ free\ water}) = G(H_2)_{water} \times D \times m_{water}$$

16 Where $G(H_2)_{water} = 4.46 \times 10^{-8}$ mol/J [LaVerne 2009]; D is the integrated dose (491.2 or
 17 997.5 kGy) and m_{water} is the total water mass (expressed in kg) present in the sample
 18 considered.

19 Finally, a first trapping efficiency parameter $TE_{free\ water}$ (expressed in % mol trapped H₂) is
 20 deduced, by comparison with free water hydrogen production, as:

$$21 \quad TE_{free\ water} = 100 \times \frac{n(H_{2\ free\ water}) - n(H_{2\ mortar\ with\ getter})}{n(H_{2\ free\ water})}$$

1 Where $n(H_{2 \text{ mortar with getter}})$ is the amount (in mol) of H₂ released by the mortar made
2 with getter. If no H₂ is released by a mortar made with getter compared to free water, the
3 corresponding value of $TE_{free \text{ water}}$ is 100%.

4 A second trapping efficiency parameter is also deduced by comparing the amounts of H₂
5 released by MnO₂-added mortars and getter-added mortars (with the same formulation), as:

$$6 \quad TE_{relative \text{ to } MnO_2} = 100 \times \frac{n(H_{2 \text{ MnO}_2}) - n(H_{2 \text{ getter}})}{n(H_{2 \text{ MnO}_2})}$$

7 Where $n(H_{2 \text{ MnO}_2})$ is the amount of H₂ produced by the γ -MnO₂-added mortar (in mol) and
8 $n(H_{2 \text{ getter}})$ is the amount of H₂ produced by the getter-added mortar (in mol). As with
9 $TE_{free \text{ water}}$, if no H₂ is released by a mortar made with getter compared to a mortar made
10 with γ -MnO₂, the corresponding value of $TE_{relative \text{ to } MnO_2}$ is 100%.

11

12 3 Results and discussion

13 Firstly, potential interactions between Portland cement paste and γ -MnO₂ or γ -MnO₂/Ag₂O
14 getter are investigated using XRD, TGA and MAS NMR for the cement solids (i.e. the Calcium
15 Aluminate and Silicate Hydrates C-A-S-H). For the getter itself, SEM/EDS analysis are
16 performed on powder grains embedded in hardened mortar. The aim is to analyze what
17 interactions exist between Portland cement paste and γ -MnO₂ or γ -MnO₂/Ag₂O.

18 Secondly, gamma Ray irradiation test results are presented and discussed. The hydrogen
19 trapping efficiency of the mortars added with getter is quantified. The impact of gamma
20 Rays on the mortar solids and pore structure is investigated by SEM observations and
21 nitrogen sorption-desorption analysis. The aim is to determine the H₂ trapping efficiency,
22 and the impact of both hydrogen trapping and gamma Ray irradiation on the mortars.

1

2 **3.1 Interactions between Portland cement pastes and γ -MnO₂ or γ -MnO₂/Ag₂O getter**

3 3.1.1 XRD results

4 The crystalline phase blend of the powders alone (γ -MnO₂ and getter), and of the Portland
5 cement pastes at identical W/C=0.5, with or without γ -MnO₂ or getter, is determined by
6 qualitative XRD (Fig. 3).

7 Fig. 3 shows that γ -MnO₂ and getter powders have very close diffractograms, except for an
8 additional peak at 33° for getter; both powders are hardly crystalline, so that phase
9 identification is not straightforward. In particular, the presence of silver carbonate Ag₂CO₃,
10 reputed favorable for trapping [Galliez 2015], is not proven.

11 For the cement pastes, the crystalline phase blend is identical with or without γ -MnO₂ or
12 getter. It comprises portlandite CH³, anhydrous crystals of hatrurite C₃S, larnite C₂S and
13 C₄AF, ettringite, quartz and mullite (the latter two are present only for Type V cement
14 paste). Being non-crystalline in commercial Portland cement paste [Lothenbach 2007,
15 Renaudin 2009], except possibly at the nanometric scale [Zhang 2000], C-A-S-H are hardly
16 distinguishable in the diffractograms. Similarly, due to slow formation kinetics, calcium
17 mono-sulfo-aluminate (or AFm for Al₂O₃-Fe₂O₃-mono) is hardly detected after 4 months
18 curing at ambient temperature (21°C), compared to calcium tri-sulfo-aluminate (i.e. AFt for
19 Al₂O₃-Fe₂O₃-tri, also ettringite) [Lothenbach 2007].

³ The typical cement notation is used here, where C stands for CaO, H for H₂O, A for Al₂O₃, S for SiO₂ and F for Fe₂O₃.

1 3.1.2 TGA analysis

2 Table 4 presents mass loss results for cement pastes made with γ -MnO₂ or γ -MnO₂/Ag₂O
3 getter, in the range of (1): 0-105°C, corresponding to the release of physi-sorbed or bound
4 water (with, in particular, ettringite decomposition), or of (2): 105-400°C, corresponding to
5 bound water release, i.e. water bound in the C-A-S-H and other more minor phases
6 [Lothenbach-2007] and of (3): 400-600°C, for portlandite Ca(OH)₂ dehydration. The mass loss
7 data are corrected for that of γ -MnO₂ or of the getter considered alone. In both cases, with
8 γ -MnO₂ or γ -MnO₂/Ag₂O, the free water release is not significantly different, whatever the
9 cement chosen (Type I or Type V), after the same maturation duration (127 days). The same
10 conclusion is drawn for bound water and for portlandite amount; there is no significant
11 difference in presence of γ -MnO₂ or γ -MnO₂/Ag₂O.

12 Therefore, from both XRD and TGA, it is concluded that the presence of getter has the same
13 impact on crystalline cement phases (and water bonding) as γ -MnO₂. Let now determine
14 exactly what impact γ -MnO₂ and γ -MnO₂/Ag₂O have on C-A-S-H.

15 3.1.3 ²⁹Si MAS NMR results

16 Figure 4 shows the ²⁹Si spectra (top) and the ²⁷Al spectra (bottom) for CEM I pastes (at
17 W/C=0.50 or 0.54, left) and for CEM V pastes (at W/C=0.50 and 0.48, right). Pastes are either
18 without addition (in blue), or with γ -MnO₂ (in green), or with γ -MnO₂/Ag₂O (in purple).

19

20 3.1.3.1- Qualitative analysis of ²⁹Si spectra

21 Let analyze these spectra first (Fig. 4 top). For both cement types, at - 69 ppm to -74 ppm,
22 the typical anhydrous phases C₂S and C₃S (belite and alite, respectively) provide rather
23 narrow peaks attributed to Q⁰ units [Bruneta 2010]. A slightly smaller amplitude of these

1 peaks is found without addition of γ -MnO₂ or getter, meaning that hydration may be slowed
2 down by γ -MnO₂ or getter. However, TGA results display no statistically significant difference
3 between γ -MnO₂ or getter (See Sub-section 3.1.2 and Table 4). It is concluded that γ -MnO₂
4 or getter have no significant impact on the hydration of Portland cement paste.

5 Moreover, for both cement types, a typical peak for Q¹-coordinated Si is located at -79 ppm,
6 whereas Q²(1Al) and Q² (i.e. Q^{2P} + Q^{2b}) resonate at -81 ppm and at -85 ppm respectively.

7 These peaks are attributed to the C-A-S-H [Andersen 2004; Chen 2004; Aono 2007; Girao
8 2007; Bach 2012; Zhang 2017].

9 For Type I pastes, for all these three peaks, no significant difference in amplitude or peak
10 position is observed with or without addition. For Type V pastes, for the Q²(1Al) and Q²
11 peaks, a slightly smaller amplitude is obtained without addition, but it is not considered
12 significant with regards to hydration phenomena (see Sub-section 3.1.2). For both Type I and
13 Type V cements, compared to the reference cement paste, no other peak on the spectra is
14 observed in presence of γ -MnO₂ or getter. It is concluded that γ -MnO₂ or getter have no
15 significant impact on the C-A-S-H structure.

16

17 3.1.3.2- Quantitative analysis of ²⁹Si spectra

18 To complete the qualitative analysis, the Q¹ and Q² contents, the mean chain length (MCL)
19 and the (Al/Si) substitution ratio are calculated for each paste and given in Table 5.

20 First, it is observed that for a given cement type, the MCL is remarkably similar whatever the
21 W/C, with values ranging between 3.3 and 3.7 for Type I Portland cement paste and 6.3 to
22 7.8 for Type V cement paste.

23 For Type I Portland cement, the MCL values at 7 days are very close to those at 127 days,
24 with less than 0.8 difference. These MCL values are similar to those determined at an

1 average of 3.3 in [Zhang 2017] for a three-year hydrated paste at W/C=0.43 (made with
2 super-plasticizer). However, for Type V Portland cement, the MCL increases significantly
3 from 7 days (with values of 3.6 to 4.4) to 127 days (with values from 6.3 to 7.8, see Table 5),
4 thanks to hydraulic or pozzolanic reactions with fly ash and blast furnace slag (initially
5 present in Type V cement). For a similar Type V/A Portland cement paste at W/C=0.39 (with
6 super-plasticizer), [Zhang 2017] determine a MCL of 21.6 after three years maturation (and
7 not only 4 months as here).

8 Moreover, the (Al/Si) molar ratios are relatively close for Type I cement pastes, with a mean
9 value of 0.040 +/-0.012 whatever the W/C and the addition. These are in good agreement
10 with values found in the literature [Skibsted 1995; Renaudin 2009; Taylor 2010; Pardal
11 2012]. The (Al/Si) values are significantly higher for Type V cement (with a mean value of
12 0.139 +/- 0.088 whatever the W/C and the addition), due to an initially greater amount of Al
13 in the cement anhydrous powder (see Table 1).

14

15 3.1.3.3- Analysis of ²⁷Al spectra

16 For ²⁷Al spectra (Fig. 4 bottom), with both cement types, the decomposition provides two
17 main peaks corresponding to Al(VI) (i.e. aluminum in an octahedric environment), at 10.2-
18 10.4 ppm (for AFm) and at 13.2-13.4 ppm (for AFt, ettringite). For Type I cement (Fig. 4 left),
19 two peaks for tetrahedric aluminum environments Al(IV) are attributed to C-A-S-H at 74.0-
20 74.3 ppm and 70.7-71.2 ppm. A small amplitude peak is at 36.5-37.7 ppm for Al(V)
21 (pentaedric aluminum, also present in the C-A-S-H). Smaller peaks at 5.2-5.4 ppm, 2.2-
22 3.1 ppm and (-4.4)-(-2.4) ppm are attributed to aluminum hydrates or hydroxides [Andersen
23 2006] or to Al(VI) inserted in the C-A-S-H inter-layer space [Mohamed 2020], or even to
24 hydrotalcite [Nguyen 2018].

1 For Type V cement (Fig. 4 bottom right), apart from AFt and AFm peaks, the second signal
2 with broader peaks at 73.5-74.1, 67.2-68.3 and 57.2-58.69 ppm are attributed to octaedric
3 Al(VI) environments due to fly ash, slag and C-A-S-H. The small amplitude peak for Al(V) is
4 also present at 36.5-37.7 ppm.

5 For both cements, the calculated percentages of AFm, AFt and aluminum hydrates (not
6 shown, see [Lanier 2020]) are not significantly different without addition, or in presence of γ -
7 MnO₂ or γ -MnO₂/Ag₂O getter.

8

9 From all these analyses, it is concluded that for both Type I and Type V cement pastes, no
10 significant difference in their phase assemblage is obtained without any addition or in
11 presence of γ -MnO₂ or getter, whether regarding the nature of the hydration products or
12 the progress of cement hydration.

13

14 **3.2 SEM observations of the getter embedded in a Portland cement mortar**

15 Let determine whether Ca sorption of the γ -MnO₂/Ag₂O getter is actually present in the
16 mortars designed and manufactured in this research (as in [Pretorius 2001]), by using
17 SEM/EDS observations.

18 Figure 5(a) is a close-up of a typical MnO₂ grain embedded in epoxy resin, before
19 incorporation into a mortar. Fig. 5(b) represents the EDS mapping of a getter grain
20 embedded in a TER-I-54 mortar sample. This shows that the getter grain presents a brim
21 enriched with Ca, as the pink color (attributed arbitrarily to Ca) highlights. Moreover, a semi-
22 quantitative EDS analysis is performed over 15 sub-areas of at least 100 μm^2 each of the
23 getter grain surface, where the atoms assumed present are Ca, Mn, C (from the epoxy resin),
24 O, and Si, yielding 100 %at. An example of an EDS spectrum obtained by this method is

1 provided in Fig. 5(c). It indicates the presence of Ca, calculated from the EDS spectra with an
2 average percentage on the order of 2.2 to 3.2 %at +/-0.5, depending on the sub-area
3 considered over the getter grain surface. The EDS analysis also demonstrates (although to a
4 lesser extent) the presence of Si inside the γ -MnO₂ grains, with a percentage of 1.2 %at +/-
5 0.5. Neither Ca nor Si were present before incorporation of γ -MnO₂ in the mortar (Fig.5(a)).
6 The presence of both atoms in the core of a getter grain might imply a limitation in the
7 trapping efficiency of the getter. Let determine their impact through gamma ray irradiation
8 tests.

9

10 **3.3 Hydrogen trapping efficiency of the Portland cement-based mortars**

11 Gamma ray irradiation tests provide *in situ* hydrogen gas from water radiolysis mechanisms.
12 Hydrogen is either trapped, or not, inside the getter-added mortars, depending on the
13 efficiency of the γ -MnO₂/Ag₂O getter. γ -MnO₂ powder is incorporated in reference mortars
14 of identical formulation, as a non-trapping powder.

15 In the following, raw results are presented, normalized and analyzed against the existing
16 literature on Portland cement-based materials. Secondly, the effect of gamma ray irradiation
17 on the pore and solid structure of each mortar is investigated, in order to determine
18 whether they are significantly affected, i.e. whether their durability may be impacted.

19 **3.3.1 Gas production after gamma ray irradiation**

20 Figure 6 displays the nitrogen and hydrogen gas volumes produced by the γ -MnO₂-based
21 mortars (Fig. 6(a)) and the getter-based mortars (Fig. 6(b)), depending on the cumulated
22 dose. In all cases, no gas other than H₂ and N₂ are detected by gas micro-chromatography;

1 CH₄, O₂, CO₂ are recorded at zero values. In particular, the absence of O₂ and CO₂ means that
2 the vial sealing has been efficient (no contact with ambient air).

3 It is also observed that for all samples, either made with γ -MnO₂ or with γ -MnO₂/Ag₂O, the
4 nitrogen production ranges between 0 and 0.5% of the gas volume available in the vial air
5 space, i.e. it is very limited. Nitrogen may originate from the degradation, due to gamma
6 rays, of the milling agent present in the Portland cement powder (its exact composition is
7 unknown).

8 The main interesting comparison is for the hydrogen produced either by γ -MnO₂-based
9 mortars or by getter-based mortars. For γ -MnO₂-based mortars, hydrogen represents
10 around 2% of the vial air space (at 491 kGy cumulated dose), and twice that value, 4%, for
11 about twice that cumulated dose (997.5 kGy). On the opposite, for getter-based mortars, the
12 hydrogen production is only on the order of 0.1-0.2% of the vial air space (at 491 kGy), and
13 0.2-0.7% at 997.5 kGy. In such case, the hydrogen production is so small that the difference
14 between the two cumulated doses is not statistically significant.

15 3.3.2 Hydrogen production – comparison with the literature

16 3.3.2.1- Trapped gas volume

17 In patent [Lambertin-2010], the H₂ trapping ability is assessed for a Portland cement paste
18 (at W/C = 0.6) including 30 %wt γ -MnO₂/Ag₂O getter, subjected to a 32°C cure for 14 days,
19 followed by a 60°C heat-treatment for 48h. The measurement includes an external H₂
20 source, which is progressively trapped by the getter mixed into the dried cement paste. The
21 H₂ trapping ability of this paste is of 120 cm³/g getter after 40 days in contact with H₂.

22 In the experiment performed here, Fig. 7 shows that the amount of H₂ trapped by each
23 mortar ranges between 0.605-0.761 cm³/g getter (at 491.2 kGy cumulated dose), and 1.199-

1 1.321 cm³/g getter (for the TER-V-48 mortar). On the whole, when doubling the cumulated
2 irradiation dose (from 491.2 to 997.5 kGy), the trapped H₂ volume by the Portland cement-
3 based mortars is almost doubled (it ranges from 1.73 to 1.98 times that at 491.2 kGy).
4 However, the recorded values are significantly smaller than for the cement paste in
5 [Lambertin-2010]. Indeed, in our experiment, H₂ is generated by water radiolysis in smaller
6 amounts than what is available from an external H₂ source (as in [Lambertin-2010]).
7 Moreover, in our research, no preliminary drying of the mortars (which favors trapping) is
8 performed.

9

10 3.3.2.2- Hydrogen radiolytic yield

11 Fig. 8 shows the normalized hydrogen radiolytic yield $\frac{G(H_2)_{material}}{w_{water}}$ of all the mortar samples

12 made with γ -MnO₂ or γ -MnO₂/Ag₂O getter, compared to that of pure water.

13 Mortars made with γ -MnO₂ have significant hydrogen production rates, with values ranging
14 between 3.42 and 6.87 x10⁻⁸ mol/J, depending on the mortar and on the sample considered.

15 For all samples (except for one TER-V-48, which may have leaked during the measurement
16 process), this is consistently greater than the value for pure water (4.46 x 10⁻⁸ mol/J). These

17 yield values are compared to usual ones for Portland-cement based materials from the
18 literature (see below). The smallest radiolytic yield is obtained with TER-I-54, although TER-
19 V-48 and QUAT-V-48 are close.

20 For mortars made with γ -MnO₂/Ag₂O, the hydrogen production is significantly smaller, with
21 values of 0.185 to 1.13 x10⁻⁸ mol/J, again depending on the mortar and on the sample
22 considered. Although the difference is very limited, the QUAT-V-48 mortar traps the greatest
23 amount of H₂ (i.e. it releases the smallest amount of H₂), and the TER-V-48 mortar traps the
24 smallest amount.

1 Complementarily, Fig. 9 compares the normalized radiolytic yield $\frac{G(H_2)_{material}}{w_{water}}$ of the
2 designed mortars to that of pure water, and to those found in the literature for Portland-
3 based cement pastes of various compositions, depending on their mass water content
4 w_{water} [Möckel 1982; Chartier 2017; Acher 2018].

5 As in Fig. 8, it is observed that the mortars made with γ -MnO₂ have a greater radiolytic yield
6 than pure water (between 5.35-6.87 x10⁻⁸ mol/J without the TER-V-48 outlier, compared to
7 4.46 x 10⁻⁸ mol/J for pure water). Former studies have quantified the same tendency as in
8 our research, but for Portland cement pastes, although these are made without γ -MnO₂. In
9 particular, for a white Portland cement paste with a mass water content w_{water} of 0.35,
10 [Chartier 2017] measure a radiolytic yield of 4.72 x 10⁻⁸ mol/J; greater values (up to 6 x 10⁻⁸
11 mol/J) are obtained for smaller w_{water} . In [Möckel 1982], measured values for the radiolytic
12 yield are above 8 x 10⁻⁸ mol/J, for w_{water} of 0.32-0.35. Although [Acher 2018] measures
13 smaller yields than pure water, most of the values in [Möckel 1982; Chartier 2017] are above
14 the radiolytic yield of pure water.

15

16 3.3.2.3- Understanding the radiolytic yield of Portland cement-based mortars

17 An explanation for the greater H₂ radiolytic yield of Portland cement pastes compared to
18 pure water is given in [Chupin 2017; Yin 2019; Cantarel 2020]. A significant linear energy
19 transfer (LET) from the cement paste solids to the liquids is inferred.

20 Indeed, in a Portland cement mortar, water is not homogeneously distributed; it is
21 integrated in the heterogeneous medium that is the cement paste (made of remains of
22 anhydrous cement, of C-A-S-H, CH, etc.), and also in the ITZ (Interfacial Transition Zone)
23 [Larbi 1993; Scrivener 2004], which is present between paste and aggregates. In cement
24 paste pores smaller than 15 nm, G. Scherer and co-workers [Valenza 2005; Xu 2009a; Xu

1 2009b] have shown experimentally that water is confined, with limited mobility and
2 anomalously high thermal expansion properties.

3 More directly, [Yin 2019] have subjected synthetic C-A-S-H (i.e. the main component of a
4 Portland cement paste) to gamma rays on the same Gammatec installation as in this
5 research. The molar calcium-to-silicium (C/S) ratio of the C-A-S-H ranges from 0.8 to 1.4, and
6 aluminum is absent, so that the experiment is rather on C-S-H than C-A-S-H. For all C-S-H, the
7 normalized radiolytic yield is greater than that of pure water. The authors relate the
8 radiolytic yield to the C/S ratio, to the C-S-H interlayer space, and also to the surface specific
9 area (SSA) of the C-S-H. In the C-S-H, the interlayer space corresponds to pores of 0.9 to 1.4
10 nm where a so-called crystallization water is located; due to the small pore sizes involved,
11 this water is considered located in a confined environment, i.e. in locations where water
12 radiolysis (among other phenomena [Valenza 2005; Xu 2009a; Xu 2009b]) may be strongly
13 affected.

14 Experimentally, [Yin 2019] show that the greater the interlayer space (and the SSA), the
15 greater the radiolytic yield, and the smaller the C/S ratio of the C-S-H. Whenever the C/S is
16 smaller, a smaller proportion of Ca compared to Si is present in the C-S-H, meaning that a
17 longer silicate chain of the C-S-H is involved [Haas 2012]. In other words, a greater radiolytic
18 yield is associated to a longer dreierketten-type silicate chain of the C-S-H [Geng 2017], to a
19 greater interlayer space and to a greater SSA, and the energy transfer (due to irradiation) is
20 greater from the C-A-S-H solids to confined water than in free water.

21 This is also expressed by [Chupin 2017] when stating that the greater the SSA of a porous
22 medium is, the greater its radiolytic yield is. Indeed, when a significant surface allowing
23 exchanges between solids/liquid exists, the energy transfer events (originating from the
24 gamma rays) are more numerous than in free water.

1 Let relate this analysis to the mortars tested in this research. Table 6 provides the SSA of all
2 mortars (made with γ -MnO₂ or γ -MnO₂/Ag₂O getter) measured by the BET approach, before
3 and after irradiation and at the same age. For all mortars before irradiation, the SSA ranges
4 between 5.4-5.5 m²/g (for QUAT-V-48), 6.0-6.9 m²/g (for TER-V-48) and 9.2-10.2 m²/g (for
5 TER-I-54). These values represent half the SSA of the cement paste of the [Lambertin 2010]
6 patent (the latter has a SSA of 21.9 m²/g). After irradiation, the SSA of all mortars is
7 consistently lower than before irradiation, with values ranging between 3.5-4.1 m²/g (for
8 QUAT-V-48), 3.8-4.2 m²/g (for TER-V-48) and 4.1-6.1 m²/g (for TER-I-54). The TER-I-54 mortar
9 has the greatest SSA before and after irradiation.

10 The results mean that irradiation significantly reduces the SSA of all mortars, possibly due to
11 enhanced energy transfer events (inside confined spaces present in the C-S-H). As a matter
12 of comparison, the mass loss after irradiation is very limited, of around 0.06-0.56 % (Table
13 6). The decrease in SSA is more pronounced for mortars made with getter than for those
14 made with γ -MnO₂. As discussed above, changes in the SSA are attributed to intense energy
15 transfer from the solids to the liquid (i.e. to the porewater).

16 In order to further ascertain this, it would be interesting to compare these results to the
17 same mortars made with a simulant of γ -MnO₂, e.g. with a fine inert filler powder.

18 3.3.3 Hydrogen trapping efficiency

19 Fig. 10 summarizes the trapping efficiency (TE) of all three mortars after 491.2 or 997.5 kGy
20 gamma irradiation. TE is expressed either relatively to pure (free) water (Fig. 10(a)) or
21 relatively to the same mortar made with MnO₂ (Fig. 10(b)).

22 In both cases, the trapping efficiency is of 85-92% for TER-I-54 mortar, 77-92% for TER-V-48
23 and 93.9-96.4% for QUAT-V-48 mortar. In other words, at least 77% (and as much as 96.4%)

1 of the hydrogen produced in the absence of getter is trapped when it is incorporated in the
2 mortar formulation. The mortar with the best trapping performance is the QUAT-V-48,
3 which requires the preliminary manufacturing of getter granules (out of the three mortars, it
4 is the most expensive to manufacture at an industrial scale). However, it is concluded that all
5 three mortars have an excellent trapping ability for hydrogen gas at both gamma irradiation
6 doses.

7 3.3.4 Changes in mortar microstructure after gamma ray irradiation

8 Apart from changes in the SSA, this last part investigates whether other changes in mortar
9 microstructures are observed after irradiation up to 997.5 kGy cumulated dose, which may
10 affect their durability.

11 3.3.4.1 Solid structure

12 Fig. 11(a) shows general views of a typical mortar microstructure (at a low magnification of
13 x300), on the example of TER-I-54, made with $\gamma\text{-MnO}_2/\text{Ag}_2\text{O}$ getter. The polished sample
14 surface is observed with the BSE detector, i.e. with grey levels representative of the atomic
15 number of the atoms present; the whiter grains are $\gamma\text{-MnO}_2/\text{Ag}_2\text{O}$, the large darker grey
16 areas are silica sand grains, the black areas are pores and the rest is cement paste. For TER-I-
17 54, a good spatial homogeneity of the $\gamma\text{-MnO}_2$ grains is visible on both images (Fig. 11(a)).
18 Similar results are obtained with $\gamma\text{-MnO}_2$ and for the two other TER-V-48 and QUAT-V-48
19 mortars.

20 Comparatively, Fig. 11 (b) shows the structure of the same TER-I-54 mortar after irradiation,
21 at a close magnification (x220) to that in Fig. 11(a). At that scale, no significant difference is
22 observed with the same mortar before irradiation (Fig. 11(a)). In particular, no specific
23 cracking is present (other than a very limited cracking pattern – seen there before

1 irradiation, and which is usual for SEM vacuumed samples). No other difference is noted
2 when using higher magnifications, up to x10k. It is concluded that the irradiation performed
3 does not change the general mortar structure as observed by SEM.

4 3.3.4.2 Pore structure

5 Following porosity before irradiation (see Appendix A.1) and SSA measurements (see sub-
6 section 3.4.2), the pore network of the mortars has been investigated in more detail through
7 pore size distributions (PSD) (Fig. 12). With nitrogen sorption-desorption, the same mortar
8 formulation is tested with γ -MnO₂ or with γ -MnO₂/Ag₂O getter, before and after irradiation.
9 Whatever the mortar considered, pore sizes measured by nitrogen sorption-desorption
10 range from 2-3 nm to about 150 nm. Bimodal PSD are obtained, as expected from the
11 literature for Portland cement-based materials [McDonald 2010; Scrivener 2011; Yio 2014].
12 For instance, for TER-I-54 made with γ -MnO₂ (Fig. 12(a)), the main peak pore size is of 54 +/-
13 2 nm (corresponding to pores located between C-A-S-H gel clusters [McDonald 2010;
14 Scrivener 2011; Yio 2014]), and the secondary peak is at 3.4 nm (corresponding to C-A-S-H
15 inner-cluster pores [McDonald 2010; Scrivener 2011; Yio 2014]). The main peak pore size is
16 slightly smaller for TER-V-48 (respectively for QUAT-V-48) made with γ -MnO₂, with a value
17 53 nm (resp. 50 nm). The secondary peak is at an identical value.

18 Moreover, whether the mortar is made with γ -MnO₂ or with γ -MnO₂/Ag₂O getter, no
19 significant difference in peak pore sizes is observed. After 1 MGy gamma irradiation, no
20 significant difference in peak pore sizes is observed either, for the mortars made with γ -
21 MnO₂ or with γ -MnO₂/Ag₂O getter.

22 However, for all mortars, the amplitude of the peaks is generally smaller after irradiation.

23 This means that irradiation does not affect the pore size distributions of the trapping

1 mortars, but it induces a decrease in the differential pore volume; less pore volume is
2 available after irradiation. This is consistent with the decrease in the SSA measured after
3 irradiation (Table 6). Both observations are attributed to intense energy transfer from the
4 solids to the liquid (i.e. to the porewater), particularly in nanometric sized pores.

5 4 Conclusions

6 This research has assessed the structure changes and the hydrogen trapping efficiency of
7 three novel formulations of Portland cement-based mortars, TER-I-54, TER-V-48 and QUAT-
8 V-48, incorporating a γ -MnO₂/Ag₂O getter, for improving the safety of radioactive waste
9 storage.

- 10 • By using XRD, TGA and MAS NMR of ²⁹Si and ²⁷Al nuclei, it is shown that the structure of
11 the Portland cement solids (i.e. the C-A-S-H) is not impacted by the presence of getter,
12 even after several month curing. Conversely, SEM+EDS analysis shows that calcium Ca
13 and Si (initially in the cement porewater) are present at the surface and in the core of the
14 γ -MnO₂/Ag₂O getter grains, and may reduce its trapping ability.
- 15 • After gamma irradiation, all three mortars made with γ -MnO₂ or getter powder release
16 more hydrogen gas than pure water subjected to the same integrated dose. This is
17 consistent with the literature on Portland-cement pastes, which clearly demonstrates
18 their greater hydrogen production compared to pure water, due to extensive energy
19 transfers between the paste solids (the C-A-S-H) and the water confined in its pores (in
20 particular those trapped below 15 nm pore diameter).
- 21 • No particular effect of γ -MnO₂, towards enhancing H₂ production, is identified from
22 these irradiation experiments alone.

1 • On the opposite, for mortars added with $\gamma\text{-MnO}_2/\text{Ag}_2\text{O}$ getter, trapping is significant,
2 with an efficiency ranging between 77 and 96.4%, depending on the integrated dose and
3 formulation considered. This efficiency is measured as the relative amount of H_2 trapped
4 by the monolithic mortar, compared to the amount produced with $\gamma\text{-MnO}_2$ mortars, or to
5 the amount produced by free water.

6 It is concluded that the developed mortars display excellent hydrogen trapping efficiency,
7 without any impact on their solid structure. This is favorable to their durability, from a
8 geochemistry viewpoint.

9

10 In further research, the efficiency of H_2 mitigation should be tested with much higher
11 gamma doses (>10 MGy) to assess the robustness of the Portland cement-based mortar
12 solutions. This has been published only for reference cementitious pastes (without getter or
13 MnO_2) in [Varlakov 2021].

14 Besides, it would be useful to assess the properties and the trapping efficiency of the novel
15 cement matrices at later ages, in drier conditions (i.e. at lower S_w), in varied aggressive
16 environments (e.g. due to accelerated carbonation or in presence of chemically aggressive
17 liquids), and after accidental scenarii (such as after a fire). Extending the research to actual
18 tritium trapping would also be useful for industrial applications, e.g. for the immobilization
19 of ITER tritiated waste.

20 Finally, considering tritium concern, the proposed getter can reduce T_2 or HT releases but
21 cannot prevent tritiated water to be released from the wastefoms in case of drying. This will
22 also require additional investigation.

1 Acknowledgments

2 Chevreul Institute (FR 2638), Ministère de l'Enseignement Supérieur, de la Recherche et de
3 l'Innovation, Hauts-de-France Region and FEDER are acknowledged for supporting and
4 funding partially this work.

5 This project, entitled MACH3, has been supported by the French Research Funding
6 programme PIA (Plan d'Investissement d'Avenir) and supervised by ANDRA under the Call
7 for Projects "Optimization of post-dismantling radioactive waste management".

8 The authors are grateful to Mr Laurent Leconte for technical expertise with data acquisition,
9 to Mr Thierry Dubois for technical assistance, and to Ms. Marie-Claude Willemetz for
10 performing the nitrogen sorption-desorption experiments.

11

1
2
3
4
5
6
7
8
9
10
11
12
13
14
15
16
17
18
19
20
21
22

Appendices

A.1- Materials (complements)

A.1.1- Powders. Cement pastes and mortars are made either with pure Portland cement, of reference CEMI 52.5R CE CP2 NF (Lafarge, Saint Pierre La Cour factory, France), or with composed Portland cement, of reference CEM V/A (S-V) 32.5N-LH HSR LA (CCB Cementir Holding, Gaurain-Ramecroix factory, Belgium).

The γ -MnO₂/Ag₂O getter is provided by A3I (France), with typical grain sizes $d_{10} = 4.5 \mu\text{m}$, $d_{50} = 13.7 \mu\text{m}$ and $d_{90} = 33.0 \mu\text{m}$ (Fig. 1). Its apparent density is 3.19 g/cm^3 , derived from the absolute density of MnO₂ (5.45 g/cm^3) [Green 2018], a total porosity of 84% and a pore volume of $0.13 \text{ cm}^3/\text{g}$ given by nitrogen sorption-desorption. The particle size distribution (PSD) of MnO₂ powder is characterized by $d_{10} = 3.2 \mu\text{m}$; $d_{50} = 9.8 \mu\text{m}$; $d_{90} = 18.0 \mu\text{m}$.

Both γ -MnO₂ and γ -MnO₂/Ag₂O powders have PSD similar to Type I cement ($d_{10} = 4.4 \mu\text{m}$, $d_{50} = 13.0 \mu\text{m}$ and $d_{90} = 26.3 \mu\text{m}$) and Type V cement ($d_{10} = 4.1 \mu\text{m}$, $d_{50} = 12.7 \mu\text{m}$ and $d_{90} = 46.6 \mu\text{m}$). However, their specific surface area, measured by the BET method (Table 1) is one order of magnitude greater. Their chemical composition is also given in Table 1. It shows the high purity of γ -MnO₂ and γ -MnO₂/Ag₂O powders. X-ray diffraction results of γ -MnO₂ and γ -MnO₂/Ag₂O powders indicate that both powders are poorly crystalline (see [Lanier 2020]).

A.1.2- Sand. For mortar manufacturing, a pure silica sand (SNL, Leucate, France) is used, with a standard particle size distribution (according to European standard EN196-1) characterized by sieving with $d_{10} = 0.15 \text{ mm}$, $d_{50} = 0.63 \text{ mm}$ and $d_{90} = 1.25 \text{ mm}$. Its main grain size classes are described in EN196-1, as 0.63-1.25 mm (it is the most important class in mass proportion, at 36%wt +/-1), 1.25-2.50 mm (second in mass proportion, at 20%wt +/-1),

1 0.315-0.63 mm (third in mass proportion, at 17%wt +/-2), 0.16-0.315 mm (fourth in mass
2 proportion, at 14%wt +/-1), and 0.08-0.16 mm (fifth in mass proportion, at 13% +/-1); sand
3 grains in the range 0.063-0.08 mm are neglected because they represent less than 1%wt.

4 **A.1.3- Super-plasticizer.** All mortars are made with a proportion of Master Glenium 27
5 (BASF, France) super-plasticizer, corresponding to 2%wt cement. It is a non-chlorinated
6 additive based on modified polycarboxylic ethers, chosen for its compatibility with ionizing
7 rays emitted by the waste [Kotatkova 2018].

8 **A.1.4- Reference paste material.** The Portland cement paste described in [Lambertin 2010],
9 labelled PASTE-REF-CEMI, is made with pure Type I Portland cement, water to a cement
10 mass ratio W/C of 0.6, and 30 %wt getter (Table 2). After mixing, the paste is sealed in a
11 hermetic container, cured for 14 days in an oven at 32 °C, then unsealed and oven-dried at
12 60 °C for 48 hours. For this paste, drying at 60°C is considered essential to drain the pore
13 network and allow gas transport.

14 Let analyze here the porosity differences with the trapping mortars developed herein. After
15 60°C drying, the porosity of all three trapping mortars is very similar, with values ranging
16 between 15.2 % +/-0.4 and 17.1 % +/-0.6 (Table 6). These are less than half the porosity of
17 PASTE-REF-CEMI. Given that without drying, this porosity is also partially filled with water, all
18 trapping mortars are bound to have a much more limited gas transport ability than PASTE-
19 REF-CEMI. This is assumed favorable to let H₂ gas more time to flow through and be trapped
20 by the getter present inside the mortars.

21 **A.1.5- Paste manufacturing, curing and drying.** Each paste is made with the same cement
22 mass (15g). For pastes containing γ -MnO₂ or γ -MnO₂/Ag₂O powder, the latter is added
23 during mixing (with a mechanical stirrer at 140 rpm) as a supplement to the paste, and

1 represents 10% of the total paste mass. For instance, the Type I Portland cement paste at
2 W/C=0.48 is made with 15,00 g cement, 7,20 g deionized water and 2,46 g γ -MnO₂ or getter.
3 Each paste is cured in an airtight container i.e. in endogenous conditions at a constant
4 temperature of 21°C for 127 days (4 months), in order to ensure sufficient maturation.
5 Nota: Other samples have also been tested after 7 days curing. They provide similar results
6 to those at 127 days (see [Lanier 2020]). With MAS NMR, anhydrous CEM I and CEM V
7 cement powder samples are also tested in the same conditions for comparison purposes.

8 **A.2- Classical characterization methods**

9 **A.2.1- Mortar pore structure.** For non-irradiated materials, the mortars are matured for 4
10 months, and oven-dried at 100°C until mass stabilization. The pore structure is quantified up
11 to a size of about 200 nm with nitrogen sorption-desorption isotherms, obtained with a
12 Micromeritics ASAP 2020 device, and up to a size of 1 mm with a Micromeritics Autopore IV
13 9500 Mercury Intrusion Porosimeter (MIP). Pore Size Distributions (PSD) are deduced from
14 desorption curves, for pores bigger than 3 nm, using the Barrett-Joyner-Halenda (BJH) model
15 [Rouquerol 2014]. As a matter of comparison, nitrogen experiments are also conducted for
16 the γ -MnO₂ and γ -MnO₂/Ag₂O powders.

17 After irradiation, mortar samples are retrieved, dried at 100°C until mass stabilization, and
18 tested for nitrogen sorption-desorption isotherms with the same procedure as non-
19 irradiated material (Table 6).

20 Using sample dry mass m_{dry} , sample porosity ϕ is measured as:

$$21 \quad \phi = \frac{V_{voids\ total}}{V_{sample}} = \frac{(m_{ethanol\ saturated} - m_{dry})}{\rho_{ethanol} V_{sample}}$$

22 Where V_{voids} is the voids volume, V_{sample} is sample volume (measured with a caliper to an
23 accuracy of 0.1 mm), $m_{ethanol\ saturated}$ is the ethanol saturated mass of the sample, and

1 $\rho_{ethanol}$ is ethanol volumetric mass (taken at a value of 789 kg/m³ at 20°C). For sample
2 saturation, ethanol is preferred to water or oil, because it does not significantly react with
3 Portland cement [Zhang 2011], and its viscosity is sufficiently low to allow sample saturation.

4

5 **A.2.2- SEM observations of mortars.** After 4 months endogenous curing, each mortar
6 sample for SEM analysis is oven-dried at 100°C until mass stabilization. Following that, each
7 sample is impregnated with epoxy resin (Epofix, Struers), polished until mirror surface finish
8 and coated with 20nm thick carbon. The SEM is a JEOL JSM-7800F LV with a FEG source,
9 equipped with secondary and backscattered electron detectors (SE and BSE) and coupled to
10 an Energy Dispersive Spectroscopy (EDS) detector, operated with the Aztec Oxford
11 Instruments software. The accelerating voltage is kept constant at 15kV and the working
12 distance at a constant value of 10 mm +/-0.1. For qualitative EDS analysis, the dead time is
13 kept at 30%+/-5 throughout.

14

15 **A.2.3- TGA analysis of cement pastes.** Thermogravimetry is performed from room
16 temperature to a target temperature of 1100°C, at a slow heating rate of 5°C per minute,
17 under an argon atmosphere. The device used is a SETARAM© thermal analyzer TG-92.
18 Preliminarily to testing the powdered cement pastes, the γ -MnO₂ and the getter powders
19 alone are tested. Their mass loss is deduced from that of the corresponding paste at the
20 same temperature.

21 The portlandite mass percentage is calculated from the mass loss in the temperature range
22 from 400 to 600°C [Mounanga 2003] [Stephant 2015] as:

1 Portlandite mass % = $\frac{\Delta m_{corrected}(400 - 600^{\circ}C)}{m_{initial\ sample}} * \frac{M(Ca(OH)_2)}{M(H_2O)}$

2 Where $\Delta m_{corrected}(400 - 600^{\circ}C)$ is the sample mass variation between 400 and 600°C,
3 corrected for that of the MnO₂ (or getter) alone, $m_{initial\ sample}$ is the sample initial mass,
4 $M(Ca(OH)_2)$ is portlandite molar mass and $M(H_2O)$ is water molar mass.

5

6 **A.3 Experimental protocol for gamma irradiation measurements**

7 After at least one week endogenous curing, each sample is removed from its mold and
8 placed in a sealed glass container without any further conditioning (i.e. no drying or water
9 saturation). This means that all samples are monoliths, and not crushed or powdered
10 mortars. The industrial irradiator uses a gamma ray ⁶⁰Co source, in the Gammatec facility at
11 CEA Marcoule (Fig. 2 left).

12 In order to quantify the released H₂ amounts, a waiting time of about 1.5 months (i.e. 38-42
13 days) is observed before analyzing the atmosphere of the glass container, i.e. of the gaseous
14 sky in the glass vials, by micro-gas chromatography (micro-GC), with an accuracy down to
15 micro-mol of gas, see Fig. 2 right. This waiting time corresponds to the time necessary for H₂
16 to flow out of the mortar monoliths by diffusion phenomena. Gas diffusion and permeability
17 are related phenomena in cement-based materials, in the sense that they both highly
18 depend on water saturation level S_w [Sercombe 2007].

19 Following the experiment, the amount of gas (H₂ but also O₂, CH₄ or N₂) released by the
20 samples $n(gas)$ is calculated (in mol) using the perfect gas law, from the raw gas volume
21 percentage %*vol* directly provided by micro-GC, from the gas pressure P_f (in Pa) in the vial
22 after irradiation and from the free vial volume V_{free} (expressed in m³), as [Lanier 2020]:

1
$$n(gas) = \frac{P_f \times \%vol \times V_{free}}{R \times T}$$

2 with R perfect gas constant (in J.mol⁻¹.K⁻¹) and T sample temperature in K⁻¹.

3 The gas radiolytic yield of the considered mortar (in mol/J) is then calculated as in [Chartier
4 2017] by:

5
$$G(gas)_{material} = \frac{n(gas)}{D m}$$

6 where $n(gas)$ is in mol, D is the cumulated dose in Gy, and m is the total sample mass (in
7 kg).

8

1 References

- 2 [Acher 2018] L. Acher, Etude du comportement sous irradiation gamma et électronique de
3 matrices cimentaires et de leurs hydrates constitutifs, Université Paris Saclay (Ecole
4 Polytechnique), PhD thesis (in French), 2018
- 5 [ANDRA 2009] French National Agency for Radioactive Waste Management (Agence
6 Nationale pour la gestion des Déchets Radioactifs ANDRA), National Inventory of Radioactive
7 Materials and Waste – Synthesis report (in English), available at
8 [https://inventaire.andra.fr/sites/default/files/documents/pdf/en/in_-_edition_2009_-
9 _synthesis_report.pdf](https://inventaire.andra.fr/sites/default/files/documents/pdf/en/in_-_edition_2009_-_synthesis_report.pdf), DCAI-CO-09-0051, ISSN: 1629-170X, 2009
- 10 [ANDRA 2015] French National Agency for Radioactive Waste Management (Agence
11 Nationale pour la gestion des Déchets Radioactifs ANDRA), PNGMDR 2013-2015-La Gestion
12 des Déchets Tritiés Liquides et Gazeux- Etat d'avancement à fin 2013 (in French), Technical
13 report n. ANDRA.398.B., 2015
- 14 [ANDRA 2018] Andra French National Agency for Radioactive Waste Management, Rapport
15 de synthèse - Inventaire national des matières et déchets radioactifs (in French), available at
16 [https://inventaire.andra.fr/sites/default/files/documents/pdf/fr/andra-synthese-2018-
17 web.pdf](https://inventaire.andra.fr/sites/default/files/documents/pdf/fr/andra-synthese-2018-web.pdf), 2018
- 18 [AEIA 2007] AIEA, Retrieval and Conditioning of Solid Radioactive Waste from Old Facilities,
19 TECHNICAL REPORTS SERIES No. 456, 2007
- 20 [Andersen 2004] M.D. Andersen, H.J. Jakobsen, J. Skibsted, « Characterization of white
21 Portland cement hydration and the C-S-H structure in the presence of sodium aluminate by
22 ²⁷Al and ²⁹Si MAS NMR spectroscopy », *Cement and Concrete Research* 34:857-868, 2004

- 1 [Andersen 2006] M. D. Andersen, H. J. Jakobsen, J. Skibsted, A new aluminium-hydrate
2 species in hydrated Portland cements characterized by ²⁷Al and ²⁹Si MAS NMR spectroscopy,
3 *Cement and Concrete Research* 36:3 – 17, 2006
- 4 [Aono 2007] Y. Aono, F. Matsushita, S. Shibata, Y. Hama, Nano-Structural Changes of C-S-H in
5 Hardened Cement Paste during Drying at 50°C, *Jal. Adv. Concr. Tech. (Japan Concr. Inst.)*,
6 5(3):313-323, 2007
- 7 [Asmussen 2018] R. M. Asmussen, C. I. Pearce, B. W. Miller, A. R. Lawter, J. J. Neeway, W. W.
8 Lukens, M. E. Bowden, M. A. Miller, E. C. Buck, R. J. Serne, N. P. Qafoku, Getters for
9 improved technetium containment in cementitious waste forms, *Journal of Hazardous*
10 *Materials*, 341:238–247, 2018
- 11 [ASN 2010] Autorité de Sûreté Nucléaire (French Nuclear Safety Authority), Livre Blanc du
12 Tritium, Groupes de réflexion menés de mai 2008 à avril 2010 sous l'égide de l'ASN et Bilan
13 annuel des rejets de tritium pour les installations nucléaire de base de 2014 à 2018,
14 Technical report (in French), updated December 17th, 2019
- 15 [Bach 2012] T.T.H. Bach, C. Cau Dit Coumes, I. Pochard, C. Mercier, B. Revel, A. Nonat,
16 *Cement and Concrete Research*, 42:805-817, 2012
- 17 [Baroghel-Bouny 1994] V. Baroghel-Bouny, Caractérisation des pâtes de ciment et des
18 bétons, PhD thesis (in French), ENPC, Paris, 1994
- 19 [Baroghel-Bouny 2004] V. Baroghel-Bouny, Concrete design for a given structure service life
20 – durability management with regards to reinforcement corrosion and alkali–silica reaction.
21 State-of-the-art and guide for the implementation of a predictive performance approach
22 based upon durability indicators. Scientific and technical documents of AFGC (AFGC), Paris,
23 240 p., issue in French: 2004 and issue in English: 2007

- 1 [Baroghel-Bouny 2007] V. Baroghel-Bouny, Water vapour sorption experiments on hardened
2 cementitious materials. Part II: Essential tool for assessment of transport properties and for
3 durability prediction, *Cement and Concrete Research*, 36(1):123-136
- 4 [Baroghel-Bouny 2009] V. Baroghel-Bouny, T. Q. Nguyen, P. Dangla, Assessment and
5 prediction of RC structure service life by means of durability indicators and
6 physical/chemical models, *Cement and Concrete Composites*, 31(8): 522-534, 2009
- 7 [Benachour 2008] Y. Benachour, C. A. Davy, F. Skoczylas, H. Houari, Effect of a high calcite
8 filler addition upon microstructural, mechanical, shrinkage and transport properties of a
9 mortar, *Cement and Concrete Research*, 38:727–736, 2008
- 10 [Bouniol 2008] P. Bouniol, E. Bjergbakke. A comprehensive model to describe radiolytic
11 processes in cement medium. *J. Nucl. Mater.* 372 (1), 1-15 (2008).
12 <https://doi.org/10.1016/j.jnucmat.2006.10.004>
- 13 [Bourbon 2017] X. Bourbon, G. Camps, Formulation des matériaux et des solutions du projet
14 structurant sur les nouvelles matrices de conditionnement. ANDRA/FDR HAVL Argile, ANDRA
15 Technical Note (in French), RTS.NT.ASCM.17.0002, 2017
- 16 [Bruneta 2010] F. Bruneta, T. Charpentier, C. N. Chao, .Peycelon, A. Nonat, Characterization by
17 solid-state NMR and selective dissolution techniques of anhydrous and hydrated CEM V
18 cement pastes, *Cement and Concrete Research*, 40:208-219, 2010
- 19 [Cantarel 2015] V. Cantarel, F. Nouaille, A. Rooses, D. Lambertin, A. Poulesquen, F. Frizon,
20 Solidification/stabilisation of liquid oil waste in metakaolin-based geopolymer, *Journal of*
21 *Nuclear Materials*, 464:16–19, 2015
- 22 [Cantarel 2020] V. Cantarel, D. Lambertin, V. Labed, I. Yamagishi, Online measurement of the
23 atmosphere around geopolymers under gamma irradiation, *Journal of Nuclear Science and*
24 *Technology*, DOI: 10.1080/00223131.2020.1801531, (2020)

- 1 [CauDitCoumes 2014] C. Cau-Dit-Coumes, D. Lambertin, H. Lahalle, P. Antonucci, C. Cannes,
2 S. Delpech, Selection of a mineral binder with potentialities for the stabilization/
3 solidification of aluminum metal, *Journal of Nuclear Materials*, 453:31–40, 2014
- 4 [Chartier 2017] D. Chartier, J. Sanchez-Canet, L. Bessette, S. Esnouf, J.-P. Renault, «Influence
5 of formulation parameters of cement based materials towards gas production under gamma
6 irradiation», *Journal of Nuclear Materials*, 511:183-190, 2018
- 7 [Chartier 2018] D. Chartier, J. Sanchez-Canet, L. Bessette, S. Esnouf, J.-P. Renault. Influence
8 of formulation of parameters of cement-based materials towards gas production under
9 gamma irradiation, *Journal of Nuclear Materials*, 511:183-190, 2018
- 10 [Chaudron 1998] V. Chaudron, A. Laurent, F. Arnould, C. Latge, Experimental evaluation of
11 hydrogen getters as mitigation technique in a fusion reactor, 17th IEEE/NPSS Symposium on
12 fusion engineering, 1- 2:208-211, 1998
- 13 [Chen 2004] J.J. Chen, J.J. Thomas, H.F.W. Taylor, H.M. Jennings, *Cement and Concrete*
14 *Research* 34:1499-1519, 2004
- 15 [Chen 2009] X.T. Chen, Th. Rougelot, C. A. Davy, W. Chen, F. Agostini, F. Skoczylas, X.
16 Bourbon, Experimental evidence of a moisture clog effect in cement-based materials under
17 temperature, *Cement and Concrete Research*, 39:1139–1148, 2009
- 18 [Chen 2012] W. Chen, J. Liu, F. G. N. Brue, F. Skoczylas, C. A. Davy, X. Bourbon, J. Talandier,
19 Water retention and gas relative permeability of two industrial concretes, *Cement and*
20 *Concrete Research* 42:1001–1013, 2012
- 21 [Chen 2013] X. T. Chen, G. Caratini, C. A. Davy, D. Troadec, F. Skoczylas, Coupled transport
22 and pro-mechanical properties of a heat-treated mortar under confinement, *Cement and*
23 *Concrete Research* 49:10–20, 2013

- 1 [Chlique 2015] C. Chlique, D. Lambertin, K. Galliez, V. Labeled, A. Dannoux-Papin, S. Jobic, P.
2 Deniard, E. Leoni, Effect of gamma irradiation on MnO₂/Ag₂O hydrogen getter, Journal of
3 Nuclear Materials 458:162–167, 2015
- 4 [Davy 2007] C.A. Davy, F. Skoczylas, J.D. Barnichon, P. Lebon, Permeability of macro-cracked
5 argillite under confinement: gas and water testing, Phys. Chem. Earth 32:667–680, 2007
- 6 [Davy 2018] C. A. Davy, G. Hauss, B. Planel, D. Lambertin, 3D structure of oil droplets in
7 hardened geopolymer emulsions, Journal of the American Ceramic Society, 1–6, DOI:
8 10.1111/jace.16142 , 2018
- 9 [De Larrard 1999] F. De Larrard, « Concrete mixture proportioning – A scientific approach »,
10 Modern Concrete Technology Series, N.9, E & FN Spon, London, 1999
- 11 [Dullien 2012] F.A. Dullien, Porous media: fluid transport and pore structure, Academic
12 Press, 2012
- 13 [EDF 2020] Electricité de France, Official website and webpage on CO₂ emissions, available at
14 <https://www.edf.fr/en/edf/co-sub-2-sub-emissions> and
15 <https://www.eia.gov/tools/faqs/faq.php?id=74&t=11>
- 16 [Galliez 2012] K. Galliez, Etude et compréhension du piégeage irréversible de l'hydrogène à
17 l'aide d'un mélange MnO₂/Ag₂O, PhD Thesis, Nantes University, France, 2012
- 18 [Galliez 2015] K. Galliez, P. Deniard, C. Payen, D. Lambertin, F. Bart, H.-J. Koo, M.-H.
19 Whangbo, S. Jobic, Pair Distribution Function and Density Functional Theory Analyses of
20 Hydrogen Trapping by γ -MnO₂, Inorganic Chemistry, 54:1194–1196, DOI: 10.1021/ic5026334
21 , 2015
- 22 [Geng 2017] G. Geng, R. Meyers, J. Li, R. Maboudian, C. Carraro, D. A. Shapiro, P. J. M.
23 Monteiro, Aluminum-induced dreierketten chain cross-links increase the mechanical

- 1 properties of nanocrystalline calcium aluminosilicate hydrate, *Nature Scientific Reports*,
2 7:44032, DOI : 10.1038/srep44032, 2017
- 3 [Girao 2007] A.V. Girão, I.G. Richardson, C.B. Porteneuve, R.M.D. Brydson, *Composition*,
4 morphology and nanostructure of C–S–H in white Portland cement pastes hydrated at 55 °C,
5 *Cement and Concrete Research* 37:1571–1582, 2007
- 6 [Green 2018] D. Green and M. Z. Southard, *Perry's Chemical Engineers' Handbook*, 85th
7 Edition, McGraw-Hill Professional, 2018
- 8 [Haas 2012]] J. Haas, « Etude expérimentale et modélisation thermodynamique du système
9 CaO-SiO₂-(Al₂O₃)-H₂O », PhD thesis (in French), Bourgogne University, France, 2012
- 10 [Janberg 1995] K. Janberg, F. Petrucci, 1995 Proceedings of the Icem-5TH International
11 Conference Radiactive Waste Management Environmental Remediation, Berlin, 285-287,
12 1995
- 13 [Juoi 2008] J.M. Juoi, Michael I. Ojovan, W. E. Lee, Microstructure and leaching durability of
14 glass composite wastefoms for spent clinoptilolite immobilisation. *J. Nucl. Mater.* 372, 358-
15 366 (2008), doi:10.1016/j.jnucmat.2007.04.047
- 16 [Kinoshita 2013] H. Kinoshita, P. Swift, C. Utton, B. Callo-Mateo, G. Marchand, N. Collier, N.
17 Milestone, Corrosion of aluminium metal in OPC- and CAC-based cement matrices, *Cement*
18 and *Concrete Research*, 50:11-18, 2013
- 19 [Klinkenberg 1941] I.J. Klinkenberg, The permeability of porous media to liquids and gases,
20 *API Drilling and Production Practices*, 200–213, 1941
- 21 [Konecny 1993] L. Konecny, S.J. Naqvi, «The effect of different drying techniques on the pore
22 size distribution of blended cement mortars », *Cement and Concrete Research* 23:1223–
23 1228, 1993

- 1 [Korpa 2006] A. Korpa, R. Trettin, « The influence of different drying methods on cement
2 paste microstructures as reflected by gas adsorption: comparison between freeze drying (F-
3 drying), D-drying, P-drying and oven-drying methods», *Cement and Concrete Research*
4 36:634–649, 2006
- 5 [Kotatkova 2018] J. Kotatkova, Z. Hlavac, V. Rosnecky, R. Mohyla, J. Jansa, The effect of
6 superplasticizers on the properties of gamma irradiated cement pastes, *Ceramics-Silikaty*,
7 62(3):306-310, 2018
- 8 [Kozawa 1980] A. Kozawa, K. V. Kordesch, Silver catalyzed manganese dioxide hydrogen gas
9 absorber, US patent n. 4,224,384, Sept. 1980
- 10 [Kozawa 1981a] A. Kozawa and K.V. Kordesch, Silver catalyzed manganese dioxide hydrogen
11 gas absorber, US patent n. 4,252,666, 1981
- 12 [Kozawa 1981b] A. Kozawa, K. V. Kordesch, Silver-catalysed MnO₂ as hydrogen absorber,
13 *Electrochimica Acta*, 26(10):1489-1493, 1981
- 14 [Lahalle 2016] H. Lahalle, « Conditionnement de l'aluminium métallique dans les ciments
15 phospho-magnésiens », PhD thesis, Bourgogne Franche -Comté University, France, 2016
- 16 [Lambertin 2010] D. Lambertin, C. Cau-Dit-Coumes, F. Frizon, C. Jousot-Dubien, Hydrogen
17 trapping material, method of preparation and uses, World patent n. WO 2010/066811 A1,
18 2010
- 19 [Lambertin 2012] D. Lambertin, F. Frizon, F. Bart, Mg–Zr alloy behavior in basic solutions and
20 immobilization in Portland cement and Na-geopolymer with sodium fluoride inhibitor,
21 *Surface & Coatings Technology*, 206:4567–4573, 2012
- 22 [Lanier 2020] S. Lanier, Mise au point d'un mortier de piégeage à réseau poreux contrôlé,
23 PhD Thesis (in French), Ecole Centrale de Lille and Université de Lille, December 2020

- 1 [Larbi 1993] J.A. Larbi, « Microstructure of the interfacial zone around aggregate particles in
2 concrete », PhD thesis, Paris-Est University, France, HAL Id: tel-00966392, 1993
- 3 [LaVerne 2009] J. A. LaVerne, M. R. Ryan, T. Mu, Hydrogen production in the radiolysis of
4 bromide solutions, *Radiation Physics and Chemistry*, 78:1148–1152, 2009
- 5 [LeCaer 2017] S. Le Caer, L. Dezerald, K. Boukari, M. Lainé, S. Taupin, R. M. Kavanagh, C. S. N.
6 Johnston, E. Foy, T. Charpentier, K. J. Krakowiak, R. J. M. Pellenq, F. J. Ulm, G. A. Tribello, J.
7 Kohanoff, A. Saul, Production of H₂ by water radiolysis in cement paste under electron
8 irradiation: A joint experimental and theoretical study, *Cement and Concrete Research*
9 100:110–118, 2017
- 10 [Le Roy 1996] R. Le Roy, Déformations instantanées et différées des bétons à hautes
11 performances, PhD thesis (in French), ENPC, also research report LPC n. 0122, Paris, 1996
- 12 [Lothenbach 2007] B. Lothenbach, F. Winnifeld, C. Alder, E. Wieland, P. Lunk, Effect of
13 temperature on the pore solution, microstructure and hydration products of Portland
14 cement pastes, *Cement and Concrete Research*, 37:483–491, 2007
- 15 [Lousot 2006] C. Lousot, C. Pichon, P. Afanasiev, M. Vrinat, M. Pijolat, F. Valdivieso, A.
16 Chevarier, N. Millard-Pinard, P. C. Leverd, Trapping of radiolytic hydrogen by amorphous
17 cobalt oxysulfide, *Journal of Nuclear Materials* 359:238–246, 2006
- 18 [Marschall 2005] P. Marschall, S. Horseman, T. Gimmi, Characterisation of Gas Transport
19 Properties of the Opalinus Clay, a Potential Host Rock Formation for Radioactive Waste
20 Disposal, *Oil & Gas Science and Technology – Rev. IFP*, 60(1):121-139, 2005
- 21 [Martin 2019] I. Martin, C. Patapy, C. Boher, M. Cyr, Investigation of caesium retention by
22 potassium nickel hexacyanoferrate (II) in different pH conditions and potential effect on the
23 selection of storage matrix, *Journal of Nuclear Materials*, 526:151764, 2019

- 1 [Massiot 2002] D. Massiot, F. Fayon, M. Capron, I. King, S. Le Calvé, B. Alonso, J.O. Durand, B.
2 Bujoli, Z. Gan, G. Hoaston. Modelling one and two- dimensional solid-state NMR spectra,
3 *Magn. Reson. Chem.*, 40:70-76, 2002
- 4 [McDonald 2010] P.J. McDonald, V. Rodin, A. Valori, Characterization of intra- and inter-C–S–
5 H gel pore water in white cement based on an analysis of NMR signal amplitudes as a
6 function of water content, *Cement and Concrete Research*, 40:1656-1663, 2010
- 7 [Mobasher 2015] N. Mobasher, S. A. Bernal, H. Kinoshita, C. A. Sharrad, J. L. Provis, Gamma
8 irradiation resistance of an early age slag-blended cement matrix for nuclear waste
9 encapsulation, *Journal of Materials Research*, 30(9):1563-1571, 2015
- 10 [Mockel 1982] H. J. Möckel, R. H. Köster, Gas Formation During the Gamma Radiolysis of
11 Cemented Low- and Intermediate-Level Waste Products, *Nuclear Technology*, 59:3, 494-497,
12 DOI: 10.13182/NT82-A33007 , 1982
- 13 [Mohamed 2020] A. K. Mohamed, P. Moutzouri, P. Berruyer, B. J. Walder, J. Siramanont, M.
14 Harris, M. Negroni, S. C. Galmarini, S. C. Parker, K. L. Scrivener, L. Emsley, P. Bowen, The
15 Atomic-Level Structure of Cementitious Calcium Aluminate Silicate Hydrate, *J. Am. Chem.*
16 *Soc.* 142(25):11060–11071, 2020
- 17 [Mounanga 2003] P. Mounanga, “Étude expérimentale du comportement de pâtes de
18 ciment au très jeune âge : hydratation, retraits, propriétés thermophysiques”, PhD thesis,
19 Nantes University, France, 2003
- 20 [Murugesan 2013] N. Murugesan, C. Ramesh, N. Sanil, M. V. Krishnaiah, R. S. I. Sundar, V.
21 Ganesan, Proton exchange membrane-based hydrogen sensor for sodium cleaning
22 application. *Sensor. ActuatB Chem.* 182, 598–604,
23 <https://doi.org/10.1016/j.snb.2013.03.055>, 2013
- 24 [Neville 2011] A.M. Neville, *Properties of Concrete*, 5th ed., Pearson, Harlow, 2011

- 1 [Nguyen 2018] T. H. Y. Nguyen, K. Tsuchiya, D. Atarashi, « Microstructure and composition of
2 fly ash and ground granulated blast furnace slag cement pastes in 42-month cured samples
3 », *Construction and Building Materials*, 191: 114-124, 2018
- 4 [Nigrey 2000] P. J. Nigrey, “An Issue Paper on the use of Hydrogen Getters in Transportation
5 Packaging,” Sandia Technical Report SAND2000-0483, Sandia National Laboratories,
6 Albuquerque, NM, 87185, 2000
- 7 [Ojovan 2005] Ojovan, M.I. and Lee, W.E.: *An Introduction to Nuclear Waste Immobilisation*,
8 Elsevier, pp. 179–200, 2005
- 9 [Pardal 2012] X. Pardal, F. Brunet, T. Charpentier, I. Pochard, A. Nonat, « ²⁷Al and ²⁹Si Solid-
10 State NMR Characterization of Calcium-Aluminosilicate-Hydrate », *Inorganic Chemistry*,
11 51:1827-1836 (doi:10.1021/ic202124x), 2012
- 12 [Renaudin 2009] G. Renaudin, J. Russias, F. Leroux, F. Frizon, C. Cau-dit-Coumes, « Structural
13 characterization of C–S–H and C–A–S–H samples—part I: long-range order investigated by
14 Rietveld analyses », *Journal of Solid State Chemistry*, 182:3312–3319, 2009
- 15 [Richardson 1994] I.G. Richardson, A.R. Brough, G.W. Groves, C.M. Dobson, « The
16 characterization of hardened alkali-activated blast-furnace slag pastes and the nature of the
17 calcium silicate hydrate (C-S-H) phase », *Cement and Concrete Research*, 24(5):813-829,
18 1994
- 19 [Richardson 1999] I.G. Richardson, «The nature of C-S-H in hardened cements », *Cement and*
20 *Concrete Research*, 29:1131-1147, 1999
- 21 [Rouquerol 2014] J. Rouquerol, F. Rouquerol, P. Llewellyn, G. Maurin, K.S. Sing, *Adsorption*
22 *by*
23 *Powders and Porous Solids: Principles, Methodology and Applications*, Academic Press, 2014

- 1 [Roquier 2016] G. Roquier, Etude de la compacité optimale des mélanges granulaires
2 binaires : classe granulaire dominante, effet de paroi, effet de desserrement, PhD thesis,
3 Université Paris Est, France, 2016
- 4 [Scrivener 2004] K L. Scrivener, A K. Crumbie, P. Laugesen, « The Interfacial Transition Zone
5 (ITZ) Between Cement Paste and Aggregate in Concrete », *Interface Science*, 12:411–421,
6 2004.
- 7 [Scrivener 2011] K L. Scrivener, A Nonat, Hydration of cementitious materials, present and
8 future, *Cement and Concrete Research*, 41:651-665, 2011
- 9 [Sedran 2007] T. Sedran, F. De Larrard, and L. Le Guen, “Détermination de la compacité des
10 ciments et additions minérales à la sonde de Vicat,” *Bulletin des Laboratoires des Ponts et*
11 *Chaussees*, 270–271:155–163, 2007
- 12 [Sercombe 2007] J. Sercombe, R. Vidal, C. Gallé, F. Adenot, Experimental study of gas
13 diffusion in cement paste, *Cement and Concrete Research* 37: 579–588, 2007
- 14 [Shi 2006] C. Shi, A. Fernandez-Jimenez, Stabilization/solidification of hazardous and
15 radioactive wastes with alkali-activated cements, *Journal of Hazardous Materials*
16 B137:1656–1663, 2006
- 17 [Skibsted 1995] [Skibsted 1995] J. Skibsted, H.J. Jakobsen, C. Hall, « Quantification of calcium
18 phases in Portland cements by ²⁹Si MAS NMR spectroscopy», *Journal of the Chemical*
19 *Society*, 91:4423-4430, 1995
- 20 [Song 2016] Y. Song, C. A. Davy, D. Trodec, Gas Breakthrough Pressure (GBP) through
21 Claystones: Correlation with FIB/SEM Imaging of the Pore Volume, *Oil & Gas Science and*
22 *Technology – Rev. IFP Energies Nouvelles*, 71:51-67, 2016

- 1 [Song 2019] Y. Song, C. A. Davy, D. Troadec, X. Bourbon, Pore network of cement hydrates in
2 a High Performance Concrete by 3D FIB/SEM - Implications for macroscopic fluid transport,
3 *Cement and Concrete Research* 115:308–326, 2019
- 4 [Stephant 2015] S. Stephant, « Etude de l'influence de l'hydratation des laitiers sur les
5 propriétés de transfert gazeux dans les matériaux cimentaires », PhD thesis, Bourgogne
6 University, France, (2015)
- 7 [Taylor 2010] R. Taylor, I.G. Richardson, R.M.D. Brydson, « Composition and microstructure
8 of 20-year-old ordinary Portland cement–ground granulated blast-furnace slag blends
9 containing 0 to 100% slag», *Cement and Concrete Research*, 40:971-983
10 (doi:10.1016/j.cemconres.2010.02.012), 2010
- 11 [US report 2017] U.S. Environmental Protection Agency, Inventory of U.S. Greenhouse Gas
12 Emissions and Sinks: 1990-2017, Executive Summary, April 2019. Includes U.S. Territories.
- 13 [Valenza 2005] J.J. Valenza and G.W. Scherer, Evidence of anomalous thermal expansion of
14 water in cement paste, *Cement Concrete Research*, 35:57-66, 2005
- 15 [Varlakov 2021] A. Varlakov, A. Zhrebtsov, M. I. Ojovan, V. Petrov, Long-term irradiation
16 effects in cementitious systems. In: *Sustainability of Life Cycle Management for Nuclear
17 Cementation-Based Technologies*. Elsevier, Woodhead Publishing, 654 p., pp. 161-180
18 (2021). <https://doi.org/10.1016/B978-0-12-818328-1.00016-2>
- 19 [Wang 2014] W. Wang, J. Liu, F. Agostini, C. A. Davy, F. Skoczylas, D. Corvez, Durability of an
20 Ultra High Performance Fiber Reinforced Concrete (UHPFRC) under progressive aging,
21 *Cement and Concrete Research* 55:1–13, 2014
- 22 [Wang 2020] B. Wang, K. Xu, Y. Wang, Using sodium D-gluconate to suppress hydrogen
23 production in wet aluminium waste dust collection systems, *Journal of Hazardous Materials*
24 397:122780, 2020

- 1 [Xu 2009a] S. Xu, G.W. Scherer, T.S. Mahadevan, and S.H. Garofalini, Thermal Expansion of
2 Confined Water, *Langmuir*, 25 [9]:5076–5083, 2009
- 3 [Xu 2009b] S. Xu, G.C. Simmons, T.S. Mahadevan, G.W. Scherer, S.H. Garofalini, Carlos
4 Pacheco, Transport of Water in Small Pores, *Langmuir* 25 [9]:5084-5090, 2009
- 5 [Yin 2019] C. Yin, A. Dannoux-Papin, J. Haas, J.-P. Renault, Influence of calcium to silica ratio
6 on H₂ gas production in calcium silicate hydrate, *Radiation Physics and Chemistry* 162:66–71
7 (2019)
- 8 [Yio 2014] M.H.N. Yio, M.J. Mac, H.S. Wong & N.R. Buenfeld, 3D imaging of cement-based
9 materials at submicron resolution by combining laser scanning confocal microscopy with
10 serial sectioning, *Journal of Microscopy*, 258(2):151-169, 2014
- 11 [Zhang 2011] J. Zhang and G. W. Scherer, Comparison of methods for arresting hydration of
12 cement, *Cement and Concrete Research*, 41:1024–1036, 2011
- 13 [Zhang 2017] Y. Zhang, C. A. Davy, G. Tricot, C. Albert-Mercier, N. Henry, P. Bertier, F.
14 Cazaux, D. Damidot, X. Bourbon, On shrinkage and structure changes of pure and blended
15 Portland concretes, *J Am Ceram Soc.* 100:4131–4152, 2017
- 16 [Zhang 2000] X. Zhang, W. Chang, T. Zhang, C. K. Ong, Nanostructure of Calcium Silicate
17 Hydrate Gels in Cement Paste, *Journal of the American Ceramic Society*, 83(10): 2600 –
18 2604, DOI: 10.1111/j.1151-2916.2000.tb01595.x, 2004.
- 19 [Zhong 2014] Zhong, S.J., Miao, N., Liu, H.Y. Analysis and protection of dust explosion
20 accidents in aluminum magnesium metal polishing process. *Modern Occupational Safety*. 10,
21 26–29, 2014

1 **Tables**

2

Oxide \ mass %	Type I (CEMI) cement	Type V (CEMV) cement	γ -MnO ₂	γ -MnO ₂ /Ag ₂ O getter
CaO	63.88	48.24	0	0
SiO ₂	17.26	25.59	0	0
SO ₃	5.14	5.75	0.63	0
Al ₂ O ₃	3.72	8.77	0	0
Na ₂ O	3.00	0	0	0
Fe ₂ O ₃	2.79	3.13	0	0
MgO	1.90	5.20	0	0
K ₂ O	1.61	2.29	0	0
TiO ₂	0.17	0.57	0	0
MnO ₂	0.1	0.1	98.90	85.01
Ag ₂ O	0	0	0	14.97
BaO	0	0	0.32	0
SrO	0	0	0.07	0
S _{BET} (m ² /g)	2.36	2.22	77.93-80.2	57.5-59.5
S _{BJH} (m ² /g)	2.45	2.19	86.6-87.7	67.8-69.8
BJH desorption average pore diameter (nm)	N/A	N/A	6.22-6.25	6.16-6.18
Minimum-Maximum pore diameters measured by nitrogen sorption-desorption (nm)	N/A	N/A	[1.8; 141.6 +/- 4.4]	[1.7; 129 +/- 2.5]

3

4 Table 1: X ray fluorescence results, specific surface area (measured by the BET or by the BJH
5 approach) and pore size distribution (also measured by nitrogen sorption-desorption) for the
6 powders involved in this research.

7

Material name	PASTE-REF-CEMI	TER-I 54	TER-V 48	QUAT-V 48
Cement type	Type I	Type I	Type V	Type V
W/C	0.6	0.54	0.48	0.48
Water (g)	262.5	243	216	216
Cement (g)	437.5	450	450	450
γ -MnO ₂ powder (g)	300	202.5	202.5	162
γ -MnO ₂ granules (g)	-	-	-	68 g, comprising 40.5 g MnO ₂ , 15.5 g cement and 12 g water
γ -MnO ₂ (% total mortar volume)	6.3	6.8	7.0	7.1
Silica sand class (1.25mm <d≤ 2.5mm) (g)	-	945	945	877
Silica sand class (0.063mm <d≤ 0.160mm) (g)	-	202.5	202.5	243
Super-plasticizer (g)	-	9	9	9
Corresponding volume (L)	0.50	0.90	0.90	0.90
Apparent density (g/cm ³)	2.00	2.28	2.25	2.17
Total water volume (%total vol)	52.5	27	24	24
Average ASTM spread (cm)	4.5 (slump)	20.5	22.3	21.3
Vicat setting duration (and start)	N/A	7h15 (starts after 4h mixing)	9h30 (starts after 6h30 mixing)	9h (starts after 4h30 mixing)

1

2 Table 2: Formulations of the novel Portland-based mortars (named TER-I-54, TER-V-48 and
3 QUAT-V-48) designed to best comply with the industrial specifications, and their fresh state
4 properties.

Mortar name (either made with γ -MnO ₂ or with γ - MnO ₂ /Ag ₂ O getter)	Portland cement type	Maturation duration at irradiation (days)	Cumulated dose (kGy)	Duration of the irradiation tests (days)	Duration between irradiation and μ GC (days)	Cumulated age at measurement (days)
TER-I 54	Pure (Type I)	118	491.2 or 997.5	23 or 46	39	157
TER-V 48	Composed (Type V)	117	491.2 or 997.5	23 or 46	38	155
QUAT-V 48	Composed (Type V)	115	491.2 or 997.5	23 or 46	42	157

1

2 Table 3: Main characteristics of the gamma ray irradiation tests: mortar type, mortar age at

3 gamma irradiation, cumulated dose sustained (2 samples per dose), duration of the

4 irradiation tests, waiting time between irradiation and micro-Gas Chromatography (μ GC),

5 and cumulated age at gas production measurement.

6

1

Cement paste name	Maturation duration (days)	Corrected Δm between 0 and 105°C (%)	Corrected Δm between 105 and 400°C (%)	Corrected Δm between 400 and 600°C (%)	Portlandite mass % (+/-1%)
54-I-MnO ₂	127	5.9	11.4	4.8	19.9
54-I-G	127	6.6	10.4	4.9	20.3
48-V-MnO ₂	127	6.1	10.4	2.7	11.2
48-V-G	127	4.6	11.5	2.4	10.0

2

3 Table 4: TGA results for Type I cement paste at W/C=0.54 and Type V cement paste at
4 W/C=0.48 made with either γ -MnO₂ or γ -MnO₂/Ag₂O getter (labelled G). Values are given at
5 +/-1%. Corrected mass variations correspond to mass loss data accounting for the mass loss
6 of the γ -MnO₂ or getter considered alone.

1
2

Cement paste name	Anhydrous cement content (%)	Q ¹ content (%)	Q ² content (%)	Mean Chain Length (MCL)	(Al/Si)
50-I-127d	12,8	55,1	32,1	3,3	0,039
50-I-MnO₂-127d	10,8	54,0	35,2	3,4	0,042
50-I-G-127d	14,5	49,0	36,5	3,7	0,046
54-I-127d	8,5	55,6	35,9	3,4	0,040
54-I-MnO₂-127d	9,2	55,6	35,2	3,4	0,028
54-I-G-127d	11,0	51,0	38,0	3,6	0,041
50-V-127d	39,4	21,6	39,0	6,4	0,131
50-V-MnO₂-127d	39,6	21,4	39,0	6,4	0,131
50-V-G-127d	36,0	22,5	41,5	6,4	0,134
48-V-127d	31,8	24,5	43,7	6,3	0,138
48-V-MnO₂-127d	37,1	18,6	44,3	7,8	0,154
48-V-G-127d	35,5	21,6	42,9	6,8	0,146

3

4 Table 5: Computed ²⁹Si MAS NMR results providing the anhydrous cement content, the Q¹
5 and Q² content, the Mean Chain Length (MCL) of the C-A-S-H and the average (Al/Si) molar
6 ratio of the C-A-S-H (indicative of Al substitutions to Si) for Portland cement pastes made
7 with W/C=0.50 and 0.54 (Type I cement), or 0.48 and 0.50 (Type V cement), after 127 days
8 maturation in endogenous conditions. For instance, 50-I stands for W/C=0.50, Type I

9

Portland cement paste with neither γ -MnO₂ nor getter (G).

10

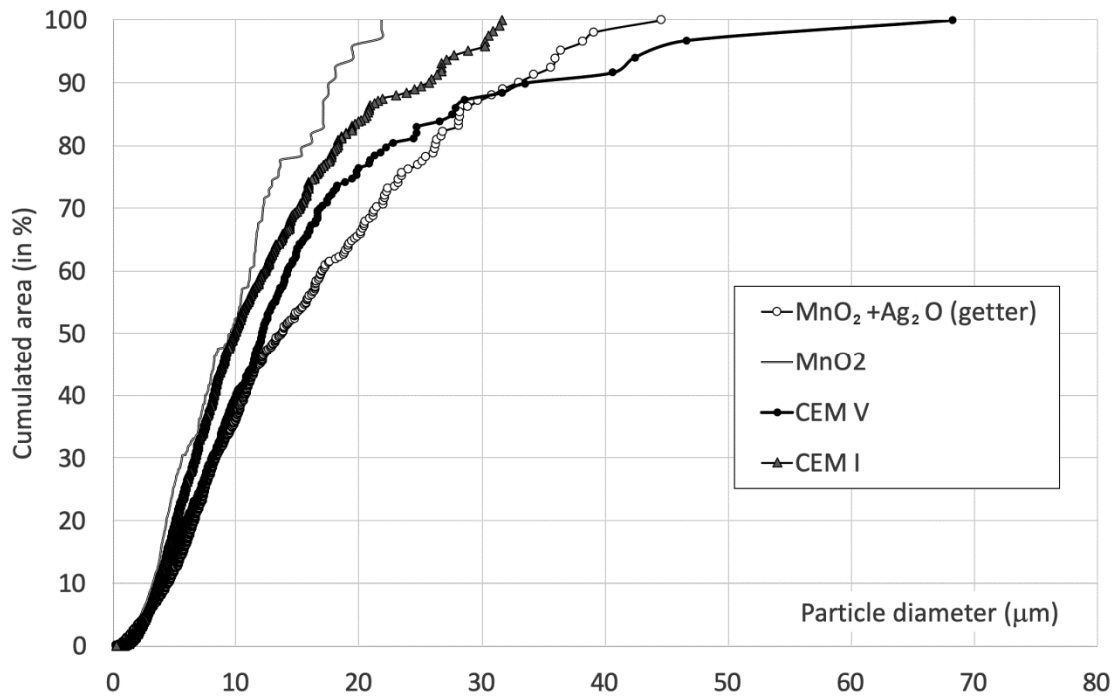
1
2

Material label	MnO ₂ or (MnO ₂ /Ag ₂ O) getter	irradiated or not	BET Specific Surface Area SSA (m ² /g)	Mass loss after irradiation (% mass before irradiation)	Porosity (%)
PASTE-REF-CEMI	getter	No	21.9	-	37.2 +/- 0.5
TER-I 54-NI	γ-MnO ₂	No	9.16	-	15.2 +/- 0.4
TER-I 54-NI	getter	No	10.17	-	-
TER-I 54-IR	γ-MnO ₂	Yes	6.13	0.08-0.16	-
TER-I 54-IR	getter	Yes	4.11	0.10-0.17	-
TER-V 48-NI	γ-MnO ₂	No	6.92	-	17.1 +/- 0.6
TER-V 48-NI	getter	No	5.99	-	-
TER-V 48-IR	γ-MnO ₂	Yes	3.84	0.08-0.18	-
TER-V 48-IR	getter	Yes	4.21	0.07-0.15	-
QUAT-V 48-NI	γ-MnO ₂	No	5.48	-	16.3 +/- 0.6
QUAT-V 48-NI	getter	No	5.38	-	-
QUAT-V 48-IR	γ-MnO ₂	Yes	4.11	0.06-0.13	-
QUAT-V 48-IR	getter	Yes	3.47	0.29-0.56	-

3
4
5
6
7
8
9

Table 6: Pore structure measurements of BET specific surface areas (by nitrogen sorption-desorption) and porosity (by ethanol saturation) for the reference cement paste from [Lambertin 2010], and for the formulated mortars with γ-MnO₂ or γ-MnO₂/Ag₂O getter. In material labels, NI stands for non irradiated and IR for irradiated; different NI and IR mortar samples are characterized at the same age, after irradiation experiments (see Table 3).

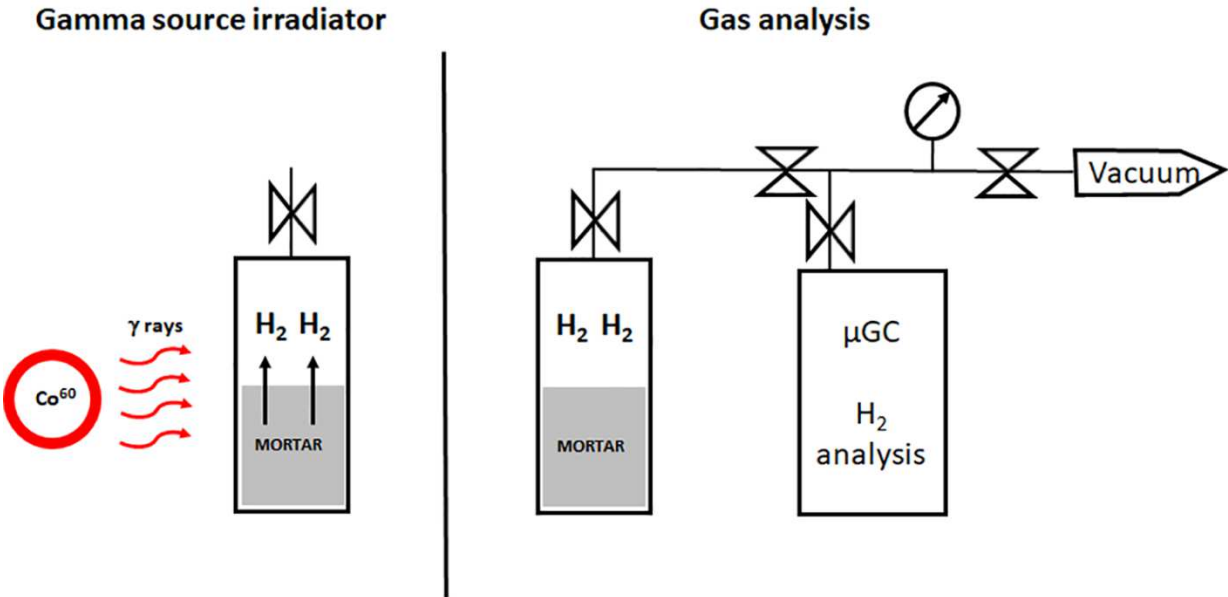
1 **Figures**



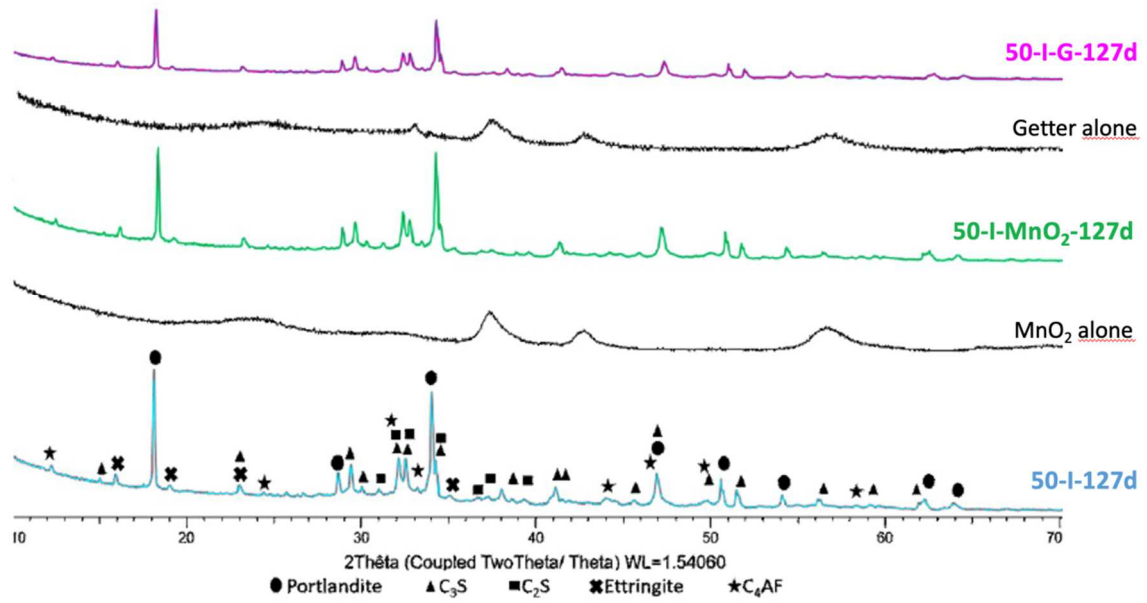
2

3 Figure 1: Grain size distributions of γ -MnO₂ (simplified as MnO₂ in the legend), γ -MnO₂/Ag₂O
 4 getter (simplified as MnO₂ + Ag₂O (getter) in the legend) and of both Type I (CEMI) and Type
 5 V (CEMV) cements.

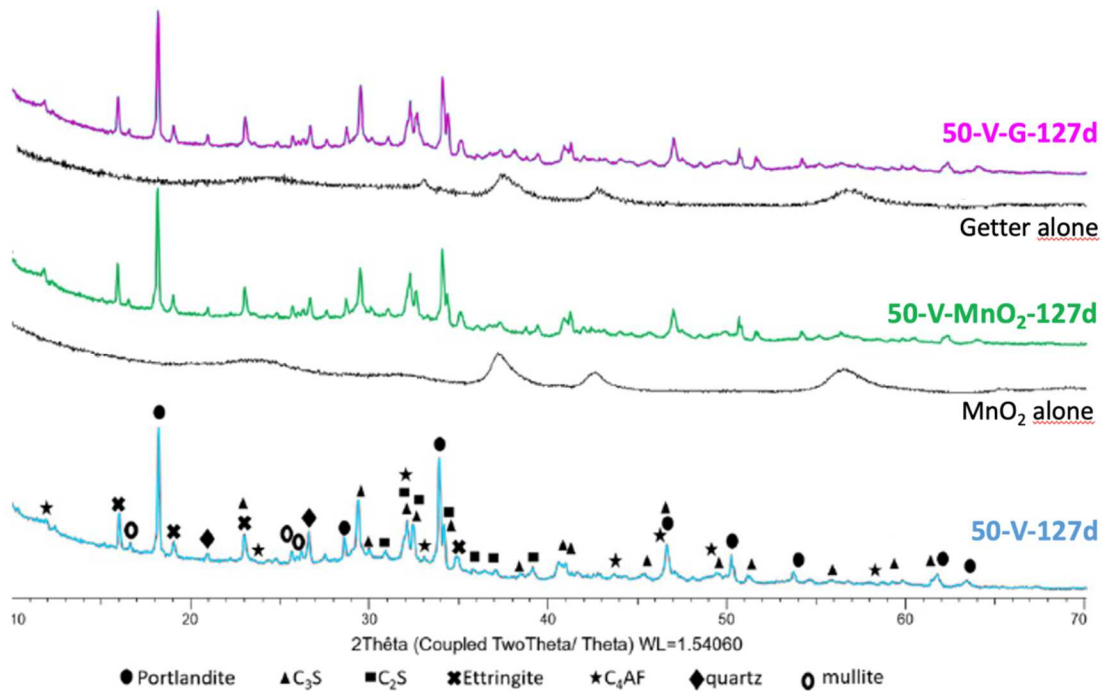
6



1
2 Figure 2: Principle of the gamma irradiation experiment using a ⁶⁰Co source. Hydrogen gas is
3 quantified by micro-Gas Chromatography (µGC).
4

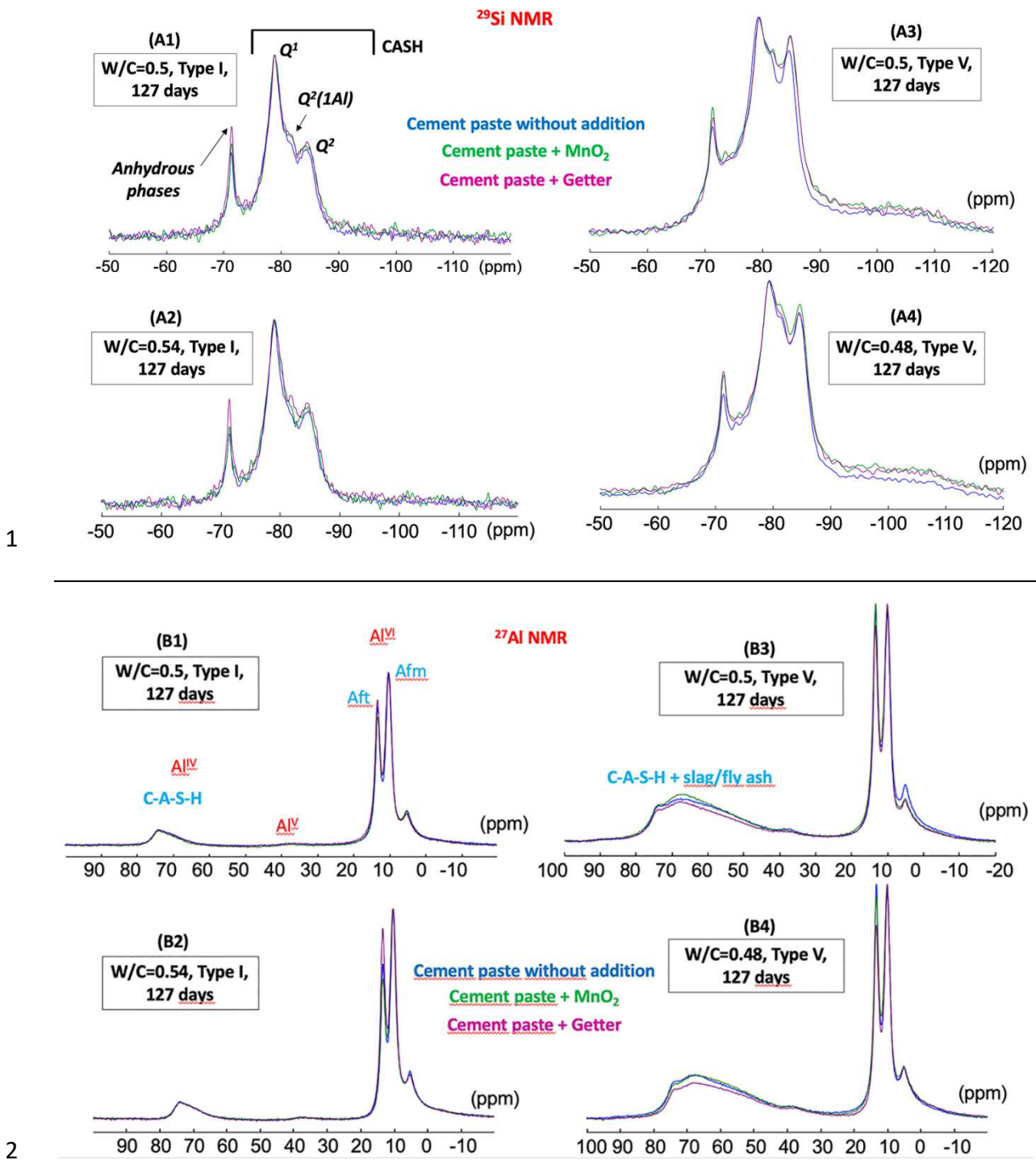


1 (a):



2 (b):

3 Figure 3: XRD results for (a): Type I and (b): Type V cement pastes at W/C=0.5, after 127 days
 4 endogenous curing at 21°C +/-1 and isopropanol drying, for samples made without or with γ -
 5 MnO₂ or getter. Phase identification provides portlandite CH (black ellipsoid marks), C₃S
 6 (black triangle marks), C₂S (black square marks), ettringite (black cross marks), C₄AF (black
 7 star marks), quartz (black diamond marks) and mullite (hollow ellipsoid marks).

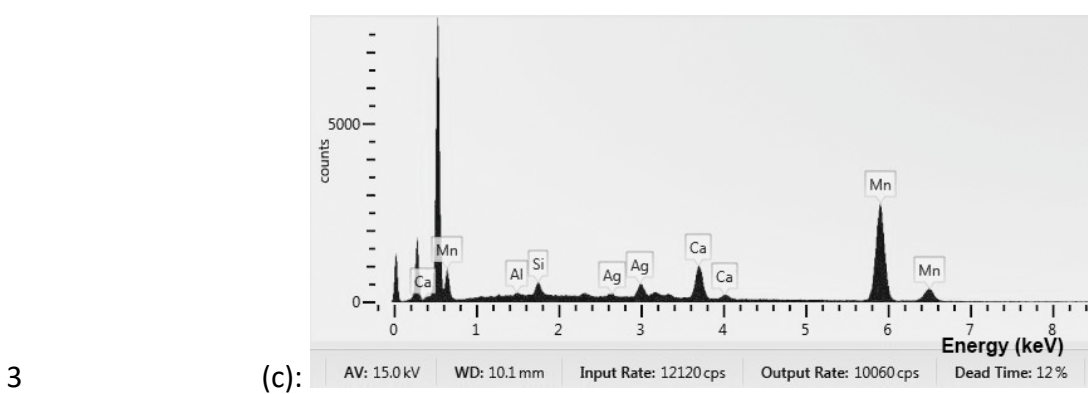
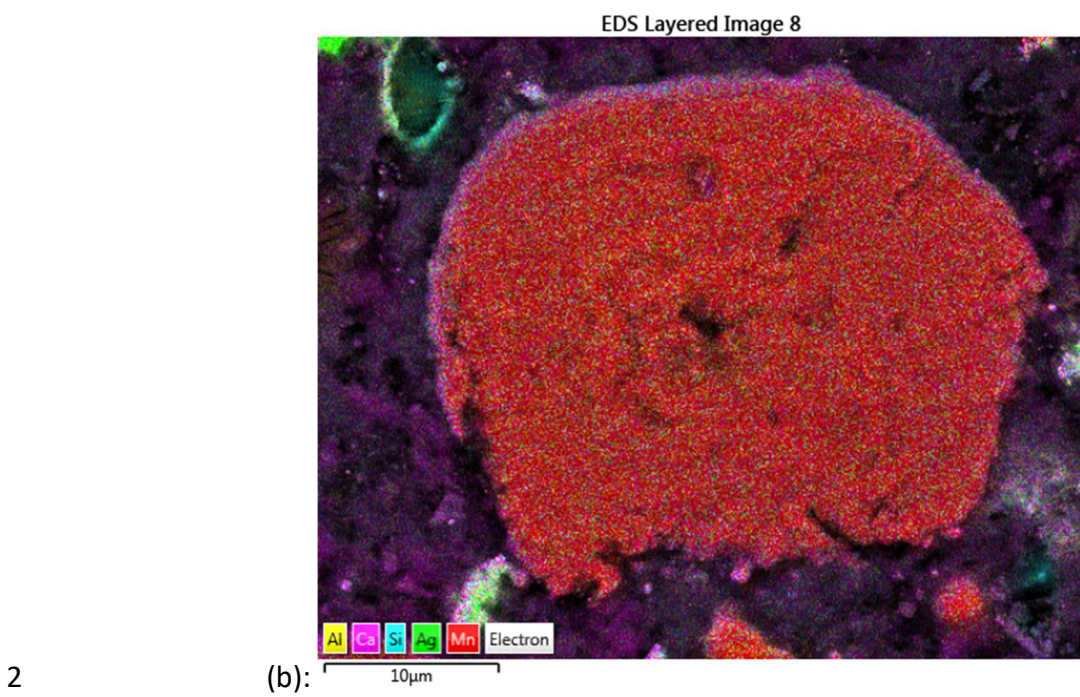
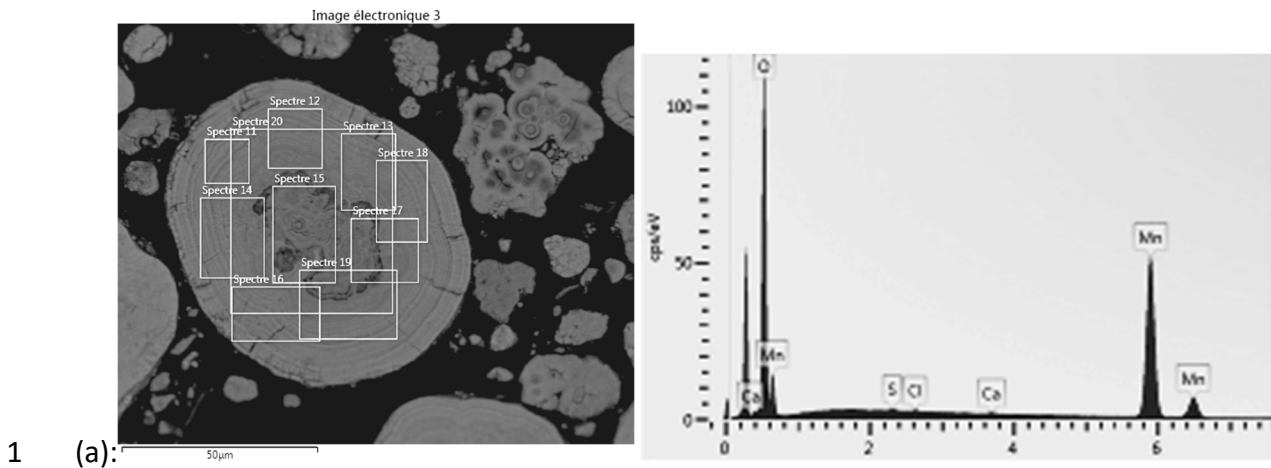


1

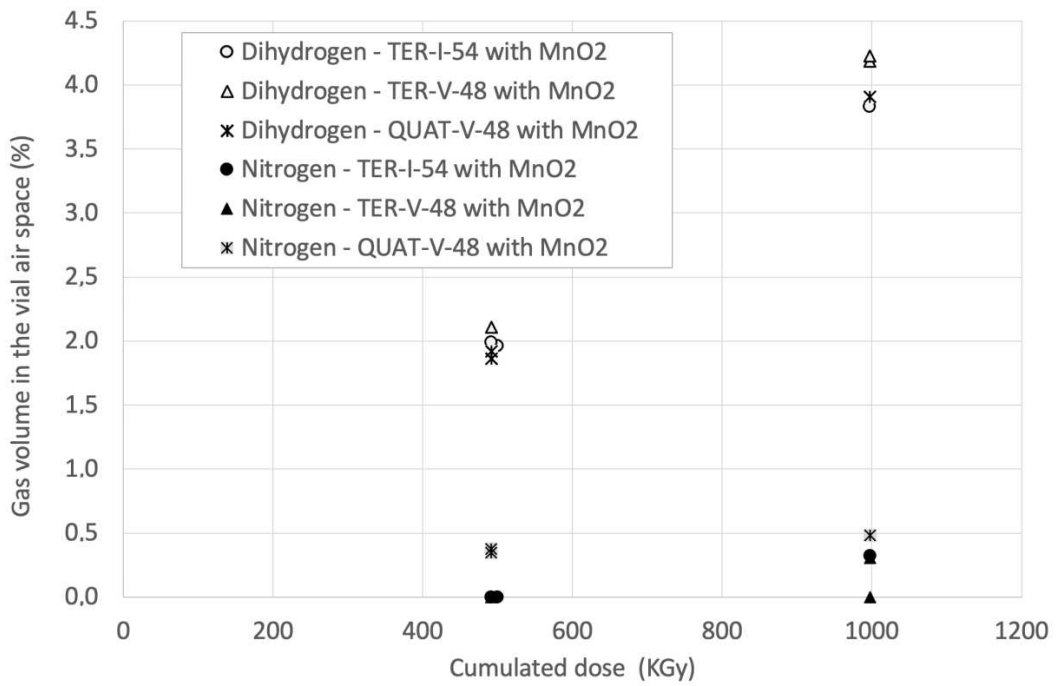
2

3 Figure 4: MAS NMR results for ^{29}Si (top graphs, labels A1 to A4) and ^{27}Al (bottom graphs,
 4 labels B1 to B4) for CEM I pastes at W/C=0.5 or 0.54 (A1, A2, B1 and B2) and CEM V pastes at
 5 W/C=0.5 or 0.48 (A3, A4, B3 and B4). Pastes are added with getter (in pink), or $\gamma\text{-MnO}_2$ (in
 6 green), or without addition (in blue).

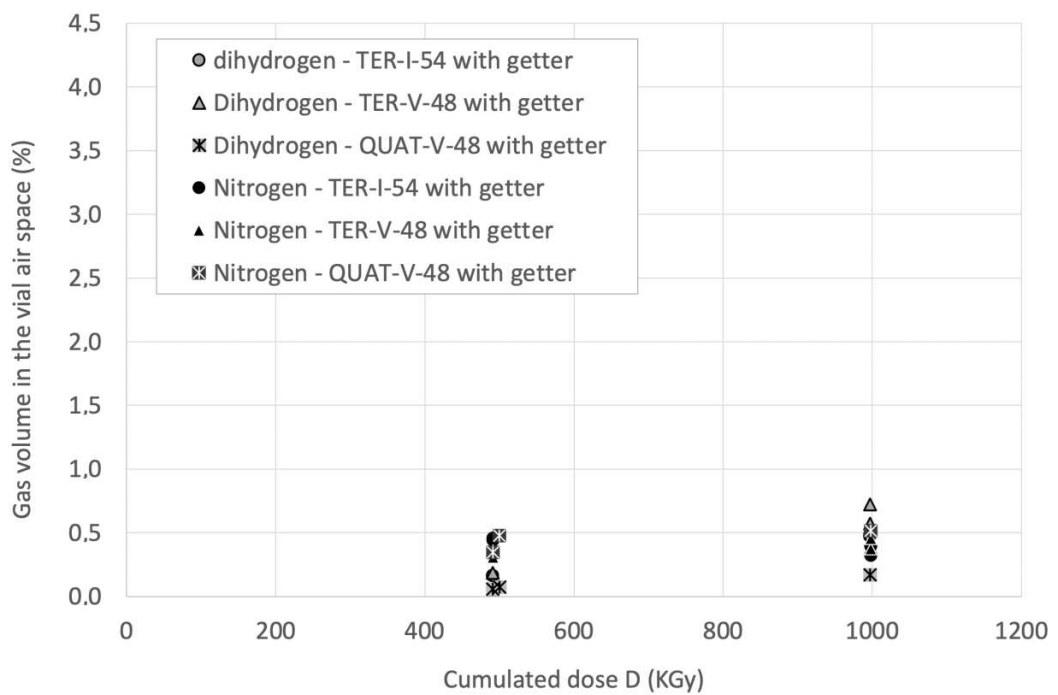
7



4 Figure 5: (a): SEM observation of a polished getter grain embedded in epoxy resin (left) and
 5 a typical EDS spectrum corresponding to the rectangular areas visible on the left; (b): SEM
 6 observation of TER-I-54 mortar (magnification x2700) and (c): Energy Dispersive
 7 Spectroscopy (EDS) cartography for Al, Ca, Si, Ag and Mn atoms performed over the whole
 8 grain area.

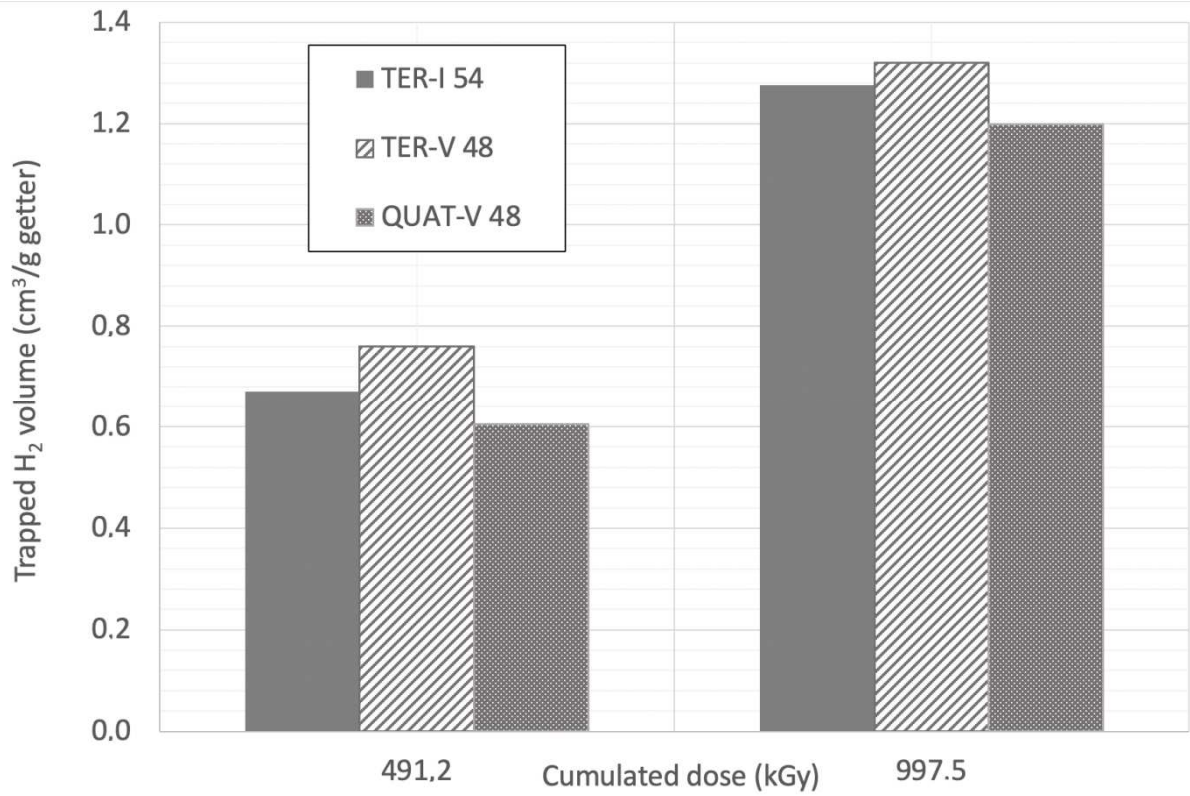


1 (a):



2 (b):

3 Figure 6: Dihydrogen and nitrogen gas volumes produced in the sample vial air space (in
 4 %vol) for each mortar sample made with (a) γ -MnO₂ or (b) getter, as a function of
 5 cumulated gamma Ray dose. Dihydrogen data points are labelled with empty circles, and
 6 nitrogen with black triangles.
 7



1

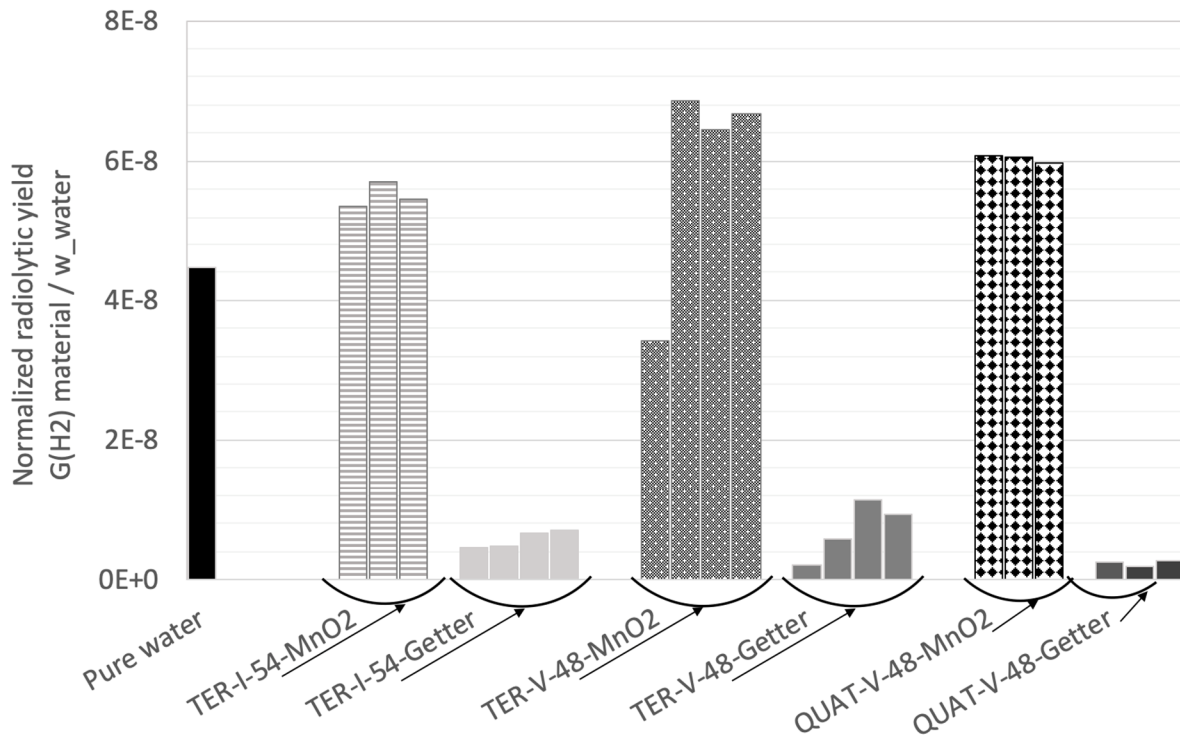
2

Figure 7: Trapped H₂ volume expressed in cm³/g getter for the three mortar formulations

3

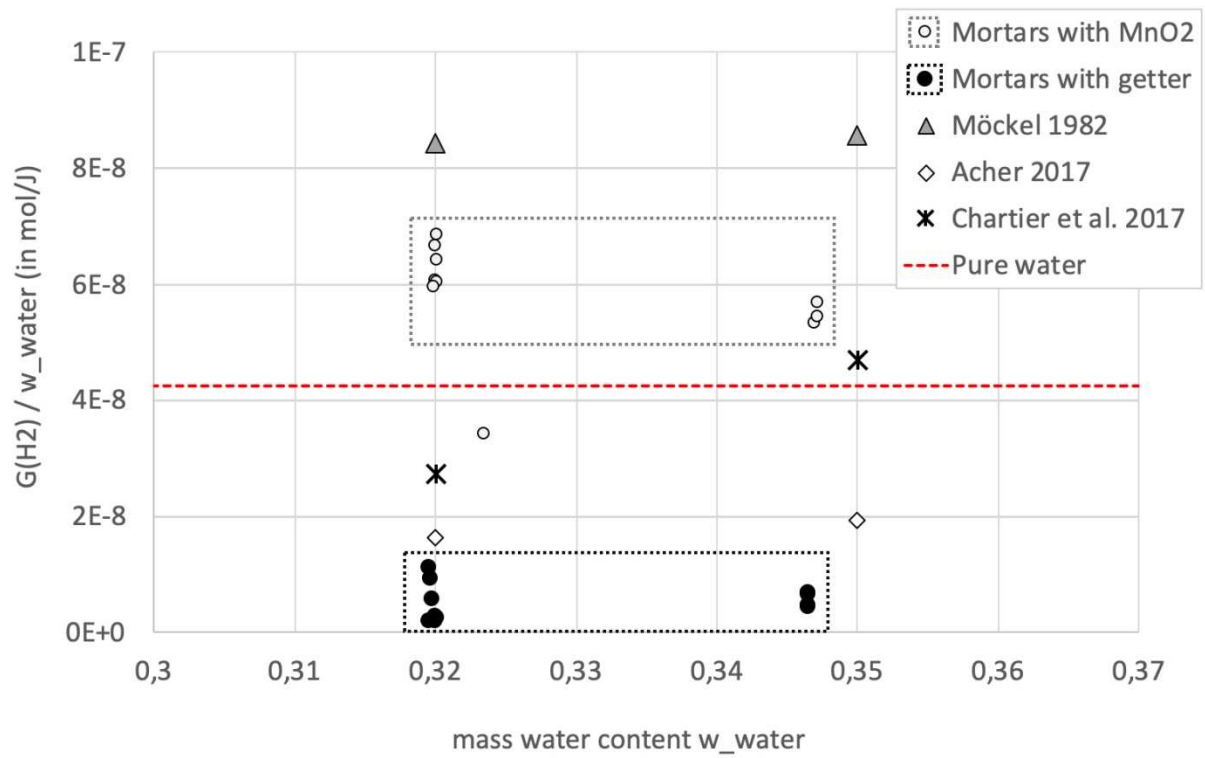
depending on the applied cumulated dose

1



2

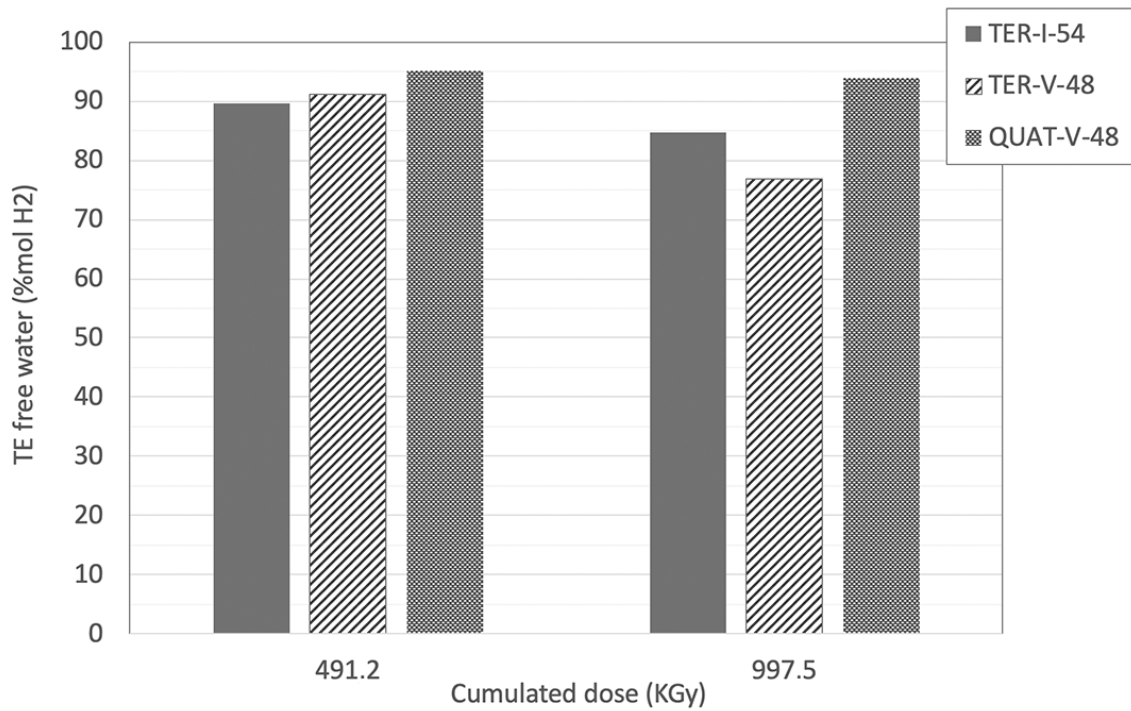
3 Figure 8: Normalized radiolytic yield $\frac{G(H_2)_{material}}{w_{water}}$ (in mol/J) for mortars made with γ -MnO₂
 4 (patterned columns) or getter (uniform columns), compared to the dihydrogen release of
 5 pure water (black column on the far left), depending on mortar formulation (TER-I-54, TER-
 6 V-48, or QUAT-V-48) and cumulated dose (per material, first two columns at 491.2 kGy, third
 7 and whenever possible fourth columns at 997.5 kGy).



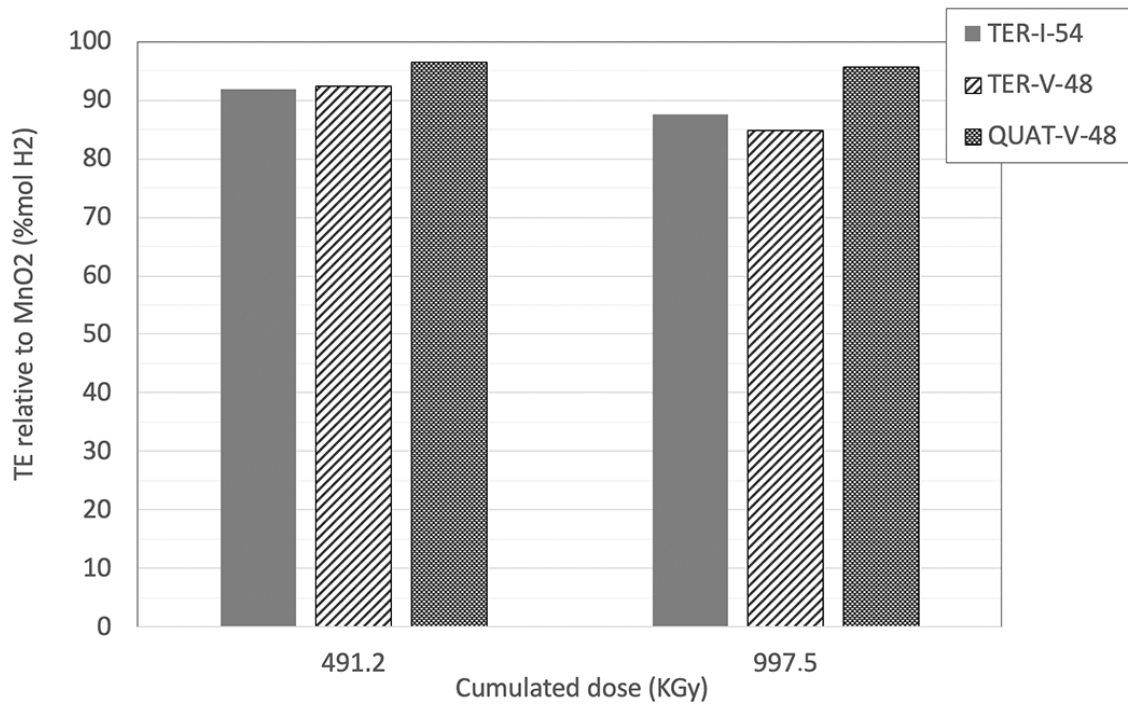
1

2 Figure 9: Normalized radiolytic yield $\frac{G(H_2)_{material}}{w_{water}}$ (in mol/J), for mortars added with γ -MnO₂
 3 or getter, compared to values in the literature for Portland cements pastes [Möckel 1982 ;
 4 Chartier 2017 ; Acher 2018] and for pure water [LaVerne 2009].

5

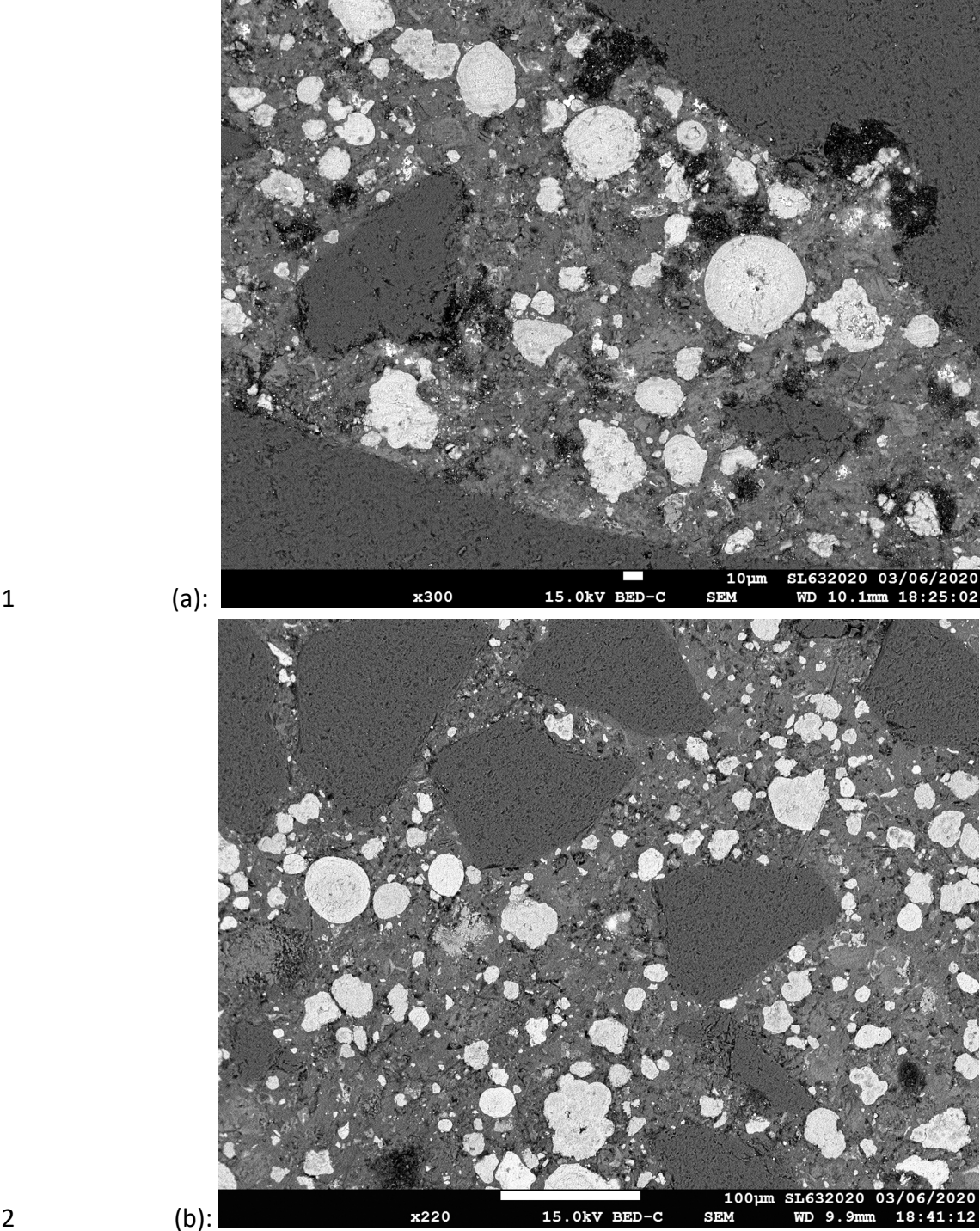


1 (a):



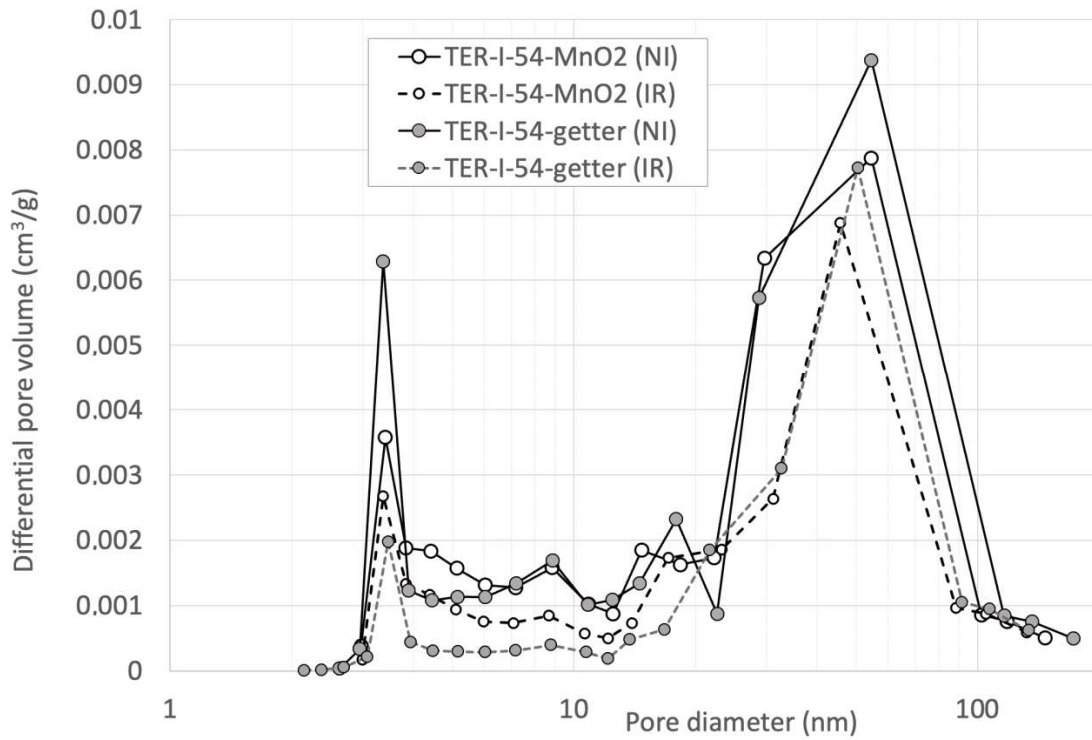
2 (b):

3 Figure 10: Dihydrogen trapping efficiency (a): $TE_{free\ water}$ (% mol H₂) and (b):
 4 $TE_{relative\ to\ MnO_2}$ for the three mortar formulations made with getter (γ -MnO₂/Ag₂O) after
 5 gamma irradiation (in kGy).

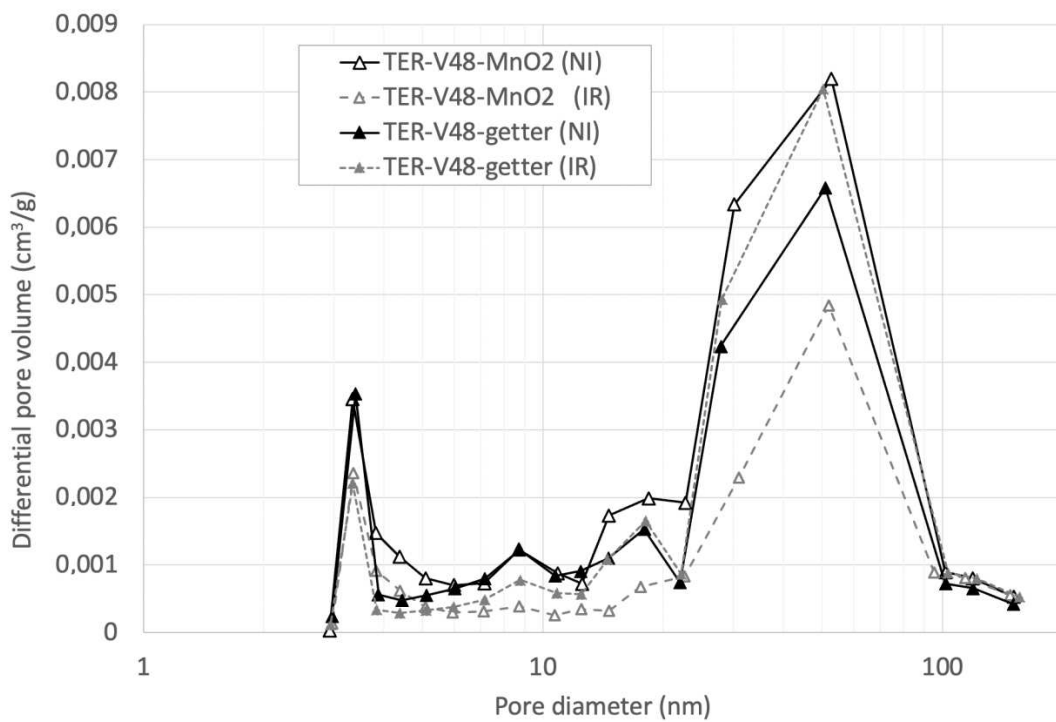


3 Figure 11: SEM observations in BSE mode of (a): TER-I-54 mortar made with γ -MnO₂/Ag₂O
4 getter before gamma irradiation (x300); (b): TER-I-54 mortar made with γ -MnO₂/Ag₂O getter
5 after gamma irradiation (x220).

1



2 (a):



3 (b):

4

5 Figure 12: Pore size distributions of trapping mortars before (NI) and after (IR) 1MGy gamma

6 irradiation, as given by nitrogen desorption for (a) TER-I-54 mortars made with γ -MnO₂ or

7 getter and (b): TER-V-48 mortars. Similar values are obtained for and QUAT-V-48 mortar.